NASA Tech Briefs

National Aeronautics and Space Administration

Electronic Components and Circuits

Electronic Systems

Physical Sciences

Materials

Computer Programs

Mechanics

Machinery

Fabrication Technology

Mathematics and Information Sciences

Life Sciences

INTRODUCTION

Tech Briefs are short announcements of innovations originating from research and development activities of the National Aeronautics and Space Administration. They emphasize information considered likely to be transferable across industrial, regional, or disciplinary lines and are issued to encourage commercial application.

Availability of NASA Tech Briefs and TSPs

Requests for individual Tech Briefs or for Technical Support Packages (TSPs) announced herein should be addressed to

National Technology Transfer Center
Telephone No. **(800) 678-6882** or via World Wide Web at **www2.nttc.edu/leads/**

Please reference the control numbers appearing at the end of each Tech Brief. Information on NASA's Commercial Technology Team, its documents, and services is also available at the same facility or on the World Wide Web at **www.nctn.hq.nasa.gov**.

Commercial Technology Offices and Patent Counsels are located at NASA field centers to provide technology-transfer access to industrial users. Inquiries can be made by contacting NASA field centers and program offices listed below.

NASA Field Centers and Program Offices

Ames Research Center
Carolina Blake
(650) 604-1754 or
cblake@mail.arc.nasa.gov

Dryden Flight Research Center
Jenny Baer-Riedhart
(661) 276-3689 or
jenny.baer-riedhart@dfrc.nasa.gov

Goddard Space Flight Center
George Alcorn
(301) 286-5810 or
galcorn@gsfc.nasa.gov

Jet Propulsion Laboratory
Merle McKenzie
(818) 354-2577 or
merle.mckenzie@jpl.nasa.gov

Johnson Space Center
Hank Davis
(281) 483-0474 or
henry.l.davis1@jsc.nasa.gov

John F. Kennedy Space Center
Jim Aliberti
(321) 867-6224 or
Jim.Aliberti-1@ksc.nasa.gov

Langley Research Center
Sam Morello
(757) 864-6005 or
s.a.morello@larc.nasa.gov

Glenn Research Center
Larry Viterna
(216) 433-3484 or
cto@grc.nasa.gov

George C. Marshall Space Flight Center
Sally Little
(256) 544-4266 or
sally.little@msfc.nasa.gov

John C. Stennis Space Center
Kirk Sharp
(228) 688-1929 or
technology@ssc.nasa.gov

NASA Program Offices
At NASA Headquarters there are seven major program offices that develop and oversee technology projects of potential interest to industry:

Carl Ray
Small Business Innovation Research Program (SBIR) & Small Business Technology Transfer Program (STTR)
(202) 358-4652 or
cray@mail.hq.nasa.gov

Dr. Robert Norwood
Office of Commercial Technology (Code RW)
(202) 358-2320 or
rnorwood@mail.hq.nasa.gov

John Mankins
Office of Space Flight (Code MP)
(202) 358-4659 or
jmankins@mail.hq.nasa.gov

Terry Hertz
Office of Aero-Space Technology (Code RS)
(202) 358-4636 or
thertz@mail.hq.nasa.gov

Glen Mucklow
Office of Space Sciences (Code SM)
(202) 358-2235 or
gmucklow@mail.hq.nasa.gov

Roger Crouch
Office of Microgravity Science Applications (Code U)
(202) 358-0689 or
rcrouch@hq.nasa.gov

Granville Paules
Office of Mission to Planet Earth (Code Y)
(202) 358-0706 or
gpaules@mtpe.hq.nasa.gov

NASA TechBriefs

National Aeronautics and Space Administration

May 2001
01-05

4

BLANK PAGE

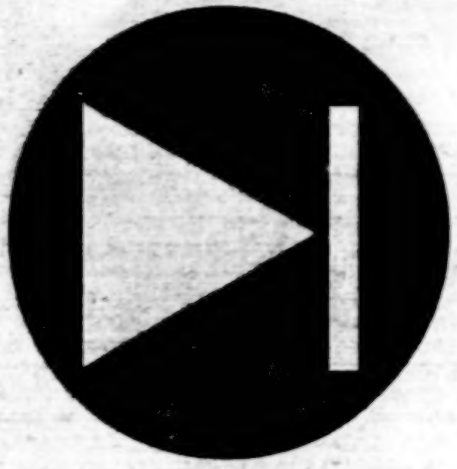

Electronic Components and Circuits

Hardware, Techniques, and Processes

6

BLANK PAGE

Simplified Construction of Conical Log-Spiral Antenna

Mating parts align themselves during assembly.

Lyndon B. Johnson Space Center, Houston, Texas

An improved design for a conical log-spiral antenna (see Figure 1) simplifies construction and improves alignment. The radiating-element substructure of such an antenna must be properly aligned with the signal-feed substructure to obtain the correct impedance match for efficient coupling of the signal into or out of the antenna. This design provides for mating parts, the faying surfaces of which enforce alignment initially during construction and maintain alignment subsequently during use.

Heretofore, the fabrication of a conical log-spiral antenna typically involved either (1) etching a sheet of metal to form the required spiral strip, then wrapping the strip around a mold or (2) manually aligning a thin, injection-molded part with a feed wire. In either case, initial alignment depends on the subjective judgement and skill of the technician, and the parts can become misaligned subsequently.

In the present improved design, the outer conical surface is a machined surface on a single-piece polytetrafluoroethylene body (see Figure 2). The use of a machined solid piece guarantees consistency of the cone angle. The inside of the body is machined to provide space for a board that holds the feed circuit, plus key slots that accept opposite edges of the board, thus aligning the feed wires with the log-spiral pattern. Instead of wrapping an etched metal spiral onto the cone, the log-spiral metal pattern is etched onto the cone before final machining.

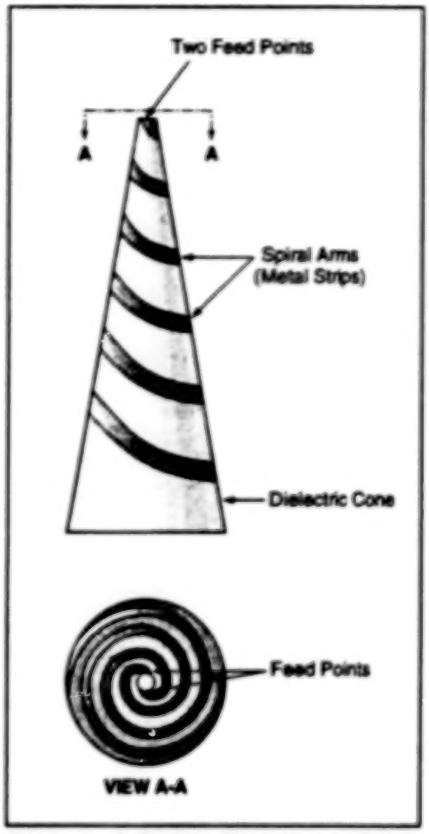

Figure 1. A Typical Conical Log-Spiral Antenna includes two spiral arms that must be kept in alignment.

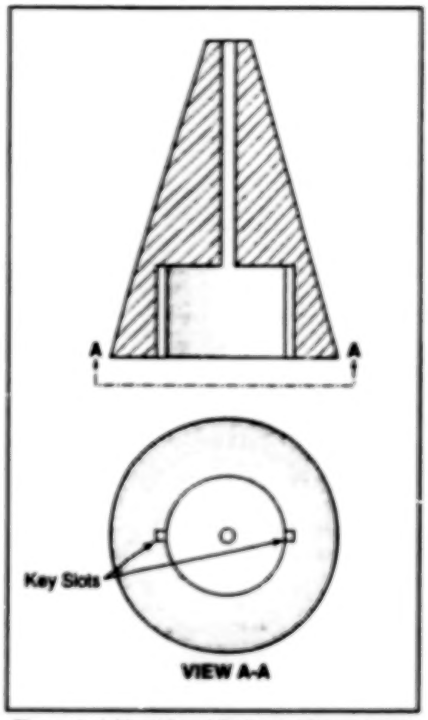

Figure 2. A Machined Polytetrafluoroethylene Body defines the spatial relationships among the spiral arms and feed wires, thereby enforcing alignment.

This work was done by Roland W. Shaw of Shason Microwave Corp. for **Johnson Space Center**. *Further information is contained in a TSP [see page 1].*
MSC-22334

High-Performance Micromachined Linear Arrays of Thermopiles

These uncooled infrared detectors can be useful in dispersive spectrometers, thermal imagers, and horizon sensors.

NASA's Jet Propulsion Laboratory, Pasadena, California

Linear arrays of thermopile infrared detectors made of high-performance thermoelectric materials have been fabricated on silicon substrates by micromachining processes. Such detector arrays can be useful in dispersive spectrometers for chemical analyses, including exhaust and environmental monitoring, in inexpensive thermal imaging systems for predictive and preventative maintenance, such as looking for hot spots on train wheels or power generating equipment, and in horizon sensors for satellite attitude control.

For some applications, thermopiles offer advantages over other uncooled infrared detectors. Thermopiles can operate over a broad temperature range without temperature stabilization. They are passive devices, generating a voltage proportional to the incident infrared power without electrical bias. They require no chopper. Thus, for some applications, thermopiles can be supported by simpler, lower-power, more-reliable ancillary components than are needed for the operation of such infrared devices as bolometers, pyroelectric or ferroelectric detectors. Another advantage is that if thermopiles are read out with high-input-impedance amplifiers, they exhibit negligible excess low-frequency (1/*f*) noise. Thermopile response is typically highly linear over many orders of magnitude in incident infrared power.

Prior to the development of the present high-performance devices, arrays of thermopiles had been fabricated by micromachining of silicon, but those arrays contained metal or silicon-based thermoelectric materials, which are characterized by low thermoelectric figures of merit. [A material's thermoelectric figure of merit is defined by $Z = \alpha^2/\rho\lambda$, where α is the Seebeck coefficient, ρ is the electrical resistivity, and λ is the thermal conductivity.] The signal-to-noise ratio of an infrared detector can be described by the specific detectivity, (D^*). The D^* of a thermopile is approximately proportional to $Z^{1/2}$.

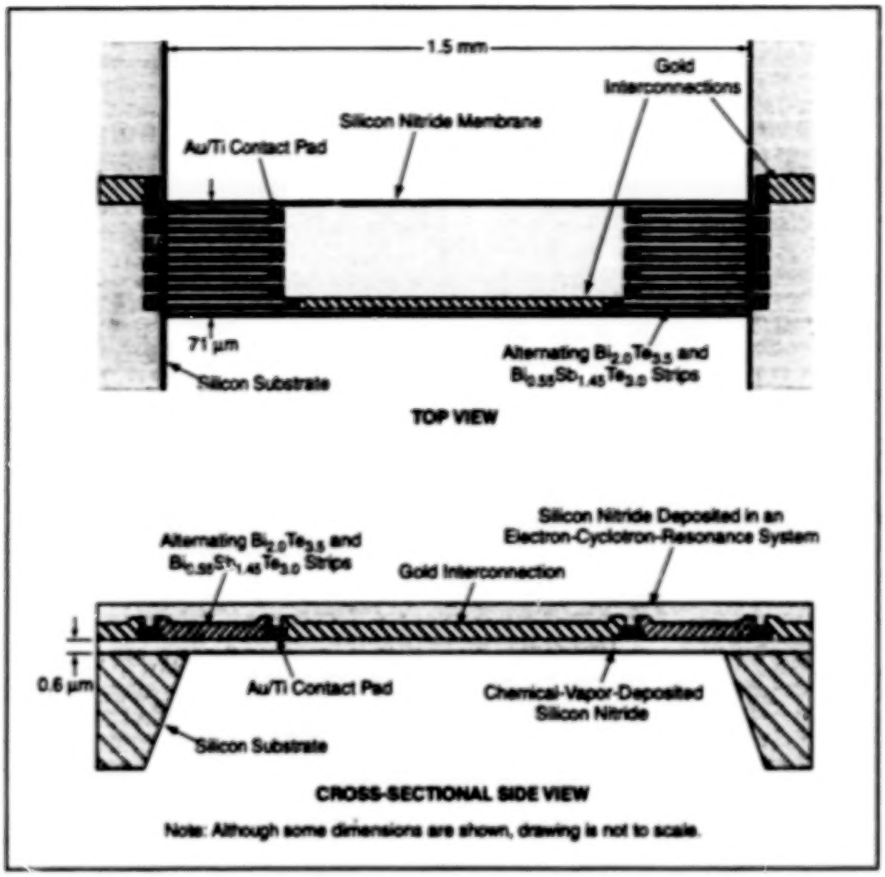

$Bi_{2.0}Te_{3.5}$/$Bi_{0.55}Sb_{1.45}Te_{3.0}$ Thin-Film Thermocouples electrically connected in series were fabricated on a silicon nitride film over a hole in a silicon substrate by standard deposition and micromachining techniques.

The present devices are 63-element linear arrays, with each element containing 11 Bi-Te/Bi-Sb-Te thin-film thermocouples, which are supported on a silicon nitride membrane over a hole in the silicon substrate to maximize the thermal isolation of the thermocouple junctions from the substrate (see figure). The thermocouple films were deposited by sputtering from targets of $Bi_{2.0}Te_{3.5}$ and $Bi_{0.55}Sb_{1.45}Te_{3.0}$. The Bi-Sb-Te-Se family of compounds has the highest known thermoelectric figure of merit at room temperature. The thin-film thermoelectric wires are electrically connected to each other and gold interconnect wiring with contact pads made of gold film deposited over titanium film.

When exposed to radiation from a 1,000 K black-body source, the detectors exhibited zero frequency responsivity values of 1,100 V/W and specific detectivities of $D^* = 1.4 \times 10^9$ cm·Hz$^{1/2}$/W, with a response time of 99 ms. The only measurable noise at frequencies above 20 mHz was Johnson noise from the detector resistance. These performance figures are the best reported to date for an array of thermopile detectors.

This work was done by Marc Foote, Eric Jones, and Thierry Caillat of Caltech for **NASA's Jet Propulsion Laboratory**.

This invention is owned by NASA, and a patent application has been filed. Inquiries concerning nonexclusive or exclusive license for its commercial development should be addressed to the Patent Counsel, NASA Management Office-JPL [see page 1]. Refer to NPO-20402.

Oscillator-Stability Analyzer Based on a Time-Tag Counter

This system would combine the best characteristics of prior single- and dual-mixer systems.

NASA's Jet Propulsion Laboratory, Pasadena, California

A proposed system for simultaneous characterization of the instability of several precise, low-noise oscillators of nominally equal frequency would be built around a commercially available time-tag counter. One of the oscillators would be deemed to be a reference oscillator, and each of the other oscillators would be compared with it by operation of a combination of hardware and software. In addition, without further modification of the hardware, any two nonreference oscillators could be compared with each other via software.

The design of the proposed stability analyzer is of a type called "dual mixer" in the precise-time-and-frequency-measurement art because the comparison of any two nonreference oscillators would involve the outputs of two mixers. There are also single-mixer stability analyzers. Single-mixer analyzers exhibit low measurement noise, but an offset-frequency reference oscillator is needed for each pair of nonreference oscillators to be compared. A prior dual-mixer analyzer contains only one offset-frequency reference oscillator, but exhibits noise greater than that of a single-mixer analyzer. The proposed system would offer both the convenience and low cost of a dual-mixer analyzer and measurement noise about as low as that of the best single-mixer analyzer.

A typical prior dual-mixer stability analyzer utilizes interpolation or extrapolation to convert several incoherent channels of beat-note zero crossings into phase residuals at a predetermined grid of times, so that the residuals of any two channels i and j can be subtracted to give an i-vs.-j comparison. This measurement is contaminated by uncanceled noise from the offset-frequency reference oscillator. The proposed system would take advantage of a modern high-rate time-tag counter to collect zero-crossing times of beat notes, the nominal frequency of which must be much greater than the desired data rate. Then the system would effect a combination of interpolation and averaging to process the time tags into low-rate phase residuals at the desired grid times. The advantage over prior art would be greater cancellation of the reference noise.

The figure schematically depicts the system. The oscillators to be compared would be of nominal frequency ν_r. The frequency of the reference oscillator would be offset by an amount ν_b. The offset reference signal would be mixed with the signal from each of the nonreference oscillators, and

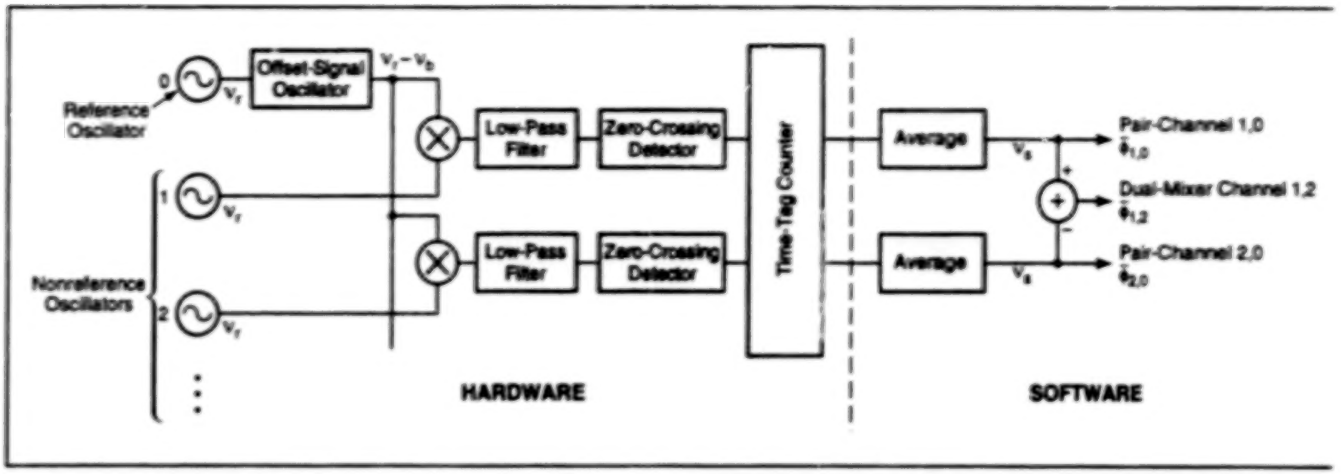

The **Dual-Mixer Stability Analyzer** would perform some of its functions in hardware and some in software. The back end of the hardware portion of the system would be a high-rate time-tag counter that would measure the times of zero crossings of beat notes.

the mixer outputs would be low-pass filtered, thereby generating beat notes of nominal frequency ν_b. By use of zero-crossing detectors, the beat notes would be converted to square-wave signals. The time-tag counter would capture the zero-crossing time tags of all the beat notes on a common time axis.

In software, the time tags would be converted to phase residuals that would be averaged over sequential intervals of duration τ_s. These intervals would be the same for all channels. The averages thus computed would constitute one of the sets of output data of the system. An essential feature of the design is that τ_s must be much greater than the beat period $\tau_b = 1/\nu_b$.

Each beat note would yield phase residuals for one pair-channel [e.g., the *i*th channel, defined with respect to the *j*th oscillator (a nonreference oscillator) vs. the zeroth oscillator (the reference oscillator)]. Because the averaging intervals would be the same for all pair-channels, the data for two pair channels could be differenced to give a synthesized dual-mixer (*i*-vs.-*j*) channel. The ability of this system to suppress the noise of the reference oscillator would depend on the relation $\tau_s >> \tau_b$.

This work was done by Charles Greenhall of Caltech for **NASA's Jet Propulsion Laboratory**. *Further information is contained in a TSP [see page 1].*
NPO-20749

BLANK PAGE

Electronic Systems

Hardware, Techniques, and Processes

BLANK PAGE

Dual-Target, Single-Laser Metrological System

It is not necessary to use two lasers with separate sets of components.

NASA's Jet Propulsion Laboratory, Pasadena, California

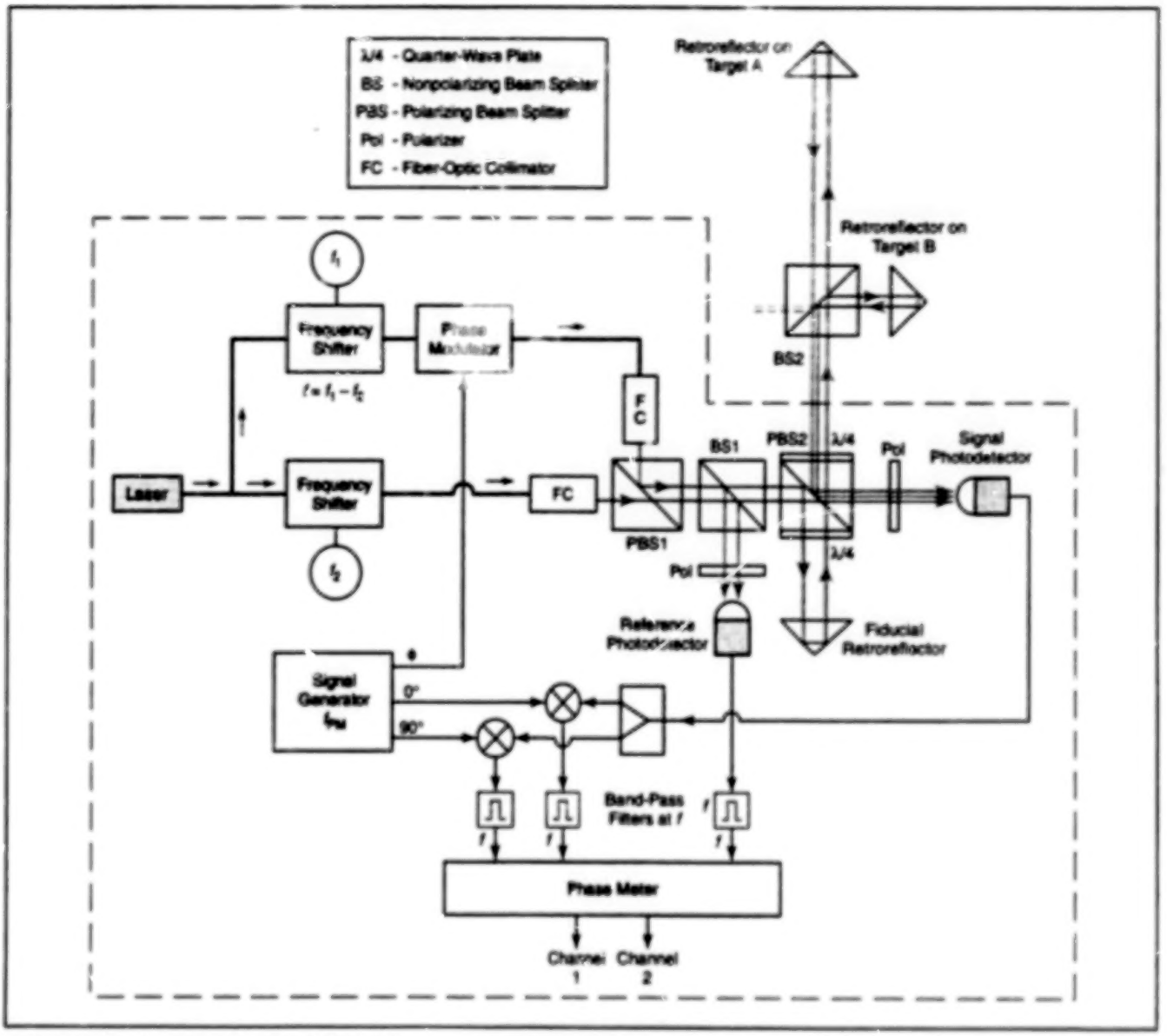

Using Only One Laser and One Set of Optical Components, the apparatus depicted schematically within the dashed outline generates separate indications of the displacements of targets A and B.

A single-laser-based, heterodyne optoelectronic system that measures the displacements of two targets along the same lines of sight has been developed. Heretofore, it would have been necessary to construct a two-target laser metrological system as two partly or wholly independent subsystems, each containing a set of optoelectronic components (including, possibly, its own laser) that must be aligned separately. The present system contains only one laser, and with the exception of the targets themselves, all optical and electronic components function together as a single system that generates a separate measurement of the displacement of each target.

More precisely, the system (see figure) measures the displacement of a retroreflector on target A and a retroreflector on target B along an optical path between each target and a fiducial retroreflector. (The portion of the optical path below beam splitter 2 in the figure is common to both targets.) Light from the single laser is launched along a single-mode optical fiber, which is split into two arms. The beams in the arms are shifted in frequency by f_1 and f_2, respectively, such that the difference frequency ($f = f_1 - f_2$) is a convenient heterodyne radio frequency. Phase modulation at radio frequency f_{PM} is applied to the f_1 arm only. The outputs of the two arms are arranged to be orthogonally polarized and collimated, and the resulting beams are combined in polarizing beam splitter 1.

The subsequent propagation of the light is very similar to that in a standard heterodyne interferometer of prior design. A small fraction of each beam is reflected by a nonpolarizing beam splitter 1, and the radio-frequency signals of the two beam fractions

are mixed in the reference photodetector. The component of the reference-photodetector output at heterodyne frequency f serves as a phase reference, against which the phases of other signal components are measured as described below.

The light transmitted by nonpolarizing beam splitter 1 enters polarizing beam splitter 2. The p-polarized light (with frequency shift f_2) is transmitted directly to the signal photodetector. The s-polarized light (with frequency shift f_1 and phase modulation at frequency f_{PM}) is reflected toward the fiducial retroreflector, from whence it is reflected back toward polarizing beam splitter 2. On its way to and from the fiducial retroreflector, this portion of the light makes a double pass through a quarter-wave plate and is thereby converted to p polarization. Now p-polarized, this portion of the light passes through polarizing beam splitter 2 and propagates to the target retroreflectors. [Although the target-B optics are shown as a combination of nonpolarizing beam splitter 2 and the target-B retroreflector, the target-B optics can also be realized as a retroreflector (only) that intercepts a fraction of same light beam that propagates toward target A.] Like the light that goes to and from the fiducial retroreflector, the light that goes to and from the targets makes a double pass through a quarter-wave plate; thus, the returns from the targets are converted back to s polarization, so that upon arrival at polarizing beam splitter 2, they are reflected toward the signal photodetector.

For each target, the output voltage of the signal photodetector includes a component

$$V_{PD,j} \propto \sin[2\pi ft + 2\pi\Delta x_j/\lambda] \sin[2\pi f_{PM}(t - \tau_j) + \phi],$$

where j represents either A or B, Δx_j is the difference between the length of the optical path from the laser straight through polarizing beam splitter 2 to the signal photodetector and the length of the optical path from the laser to target j to the signal photodetector, λ is the laser wavelength, t is the present time, τ_j is time of propagation between the phase modulator and the signal photodetector via target j, and ϕ is an adjustable constant component of the phase of the f_{PM} signal.

The output of the signal photodetector is demodulated in two channels by mixing with two differently phase-sifted versions of a signal of frequency f_{PM}, then filtering. The j component of the resulting waveform in the jth channel is given by

$$V_{demod,j} \propto \sin[2\pi ft + 2\pi\Delta x_j/\lambda] \cos[2\pi f_{PM}\tau_j - \phi - \alpha_j],$$

where α_j is a constant component of the phase of the demodulating signal of frequency f_{PM} in the jth channel ($\alpha_1 = \pi/2$, $\alpha_2 = 0$). The sine factor term is the heterodyne beat-frequency factor, the phase of which depends directly on the optical-path difference. The cosine factor establishes the amplitude of the heterodyne signal.

The waveforms in the two channels are fed to a phase meter that separately compares their phases with the phase of the output of the reference photodetector. This is the same phase-comparison process as that in a standard heterodyne laser metrological system of prior design. By choosing $\phi = 2\pi f_{PM}\tau_B$, one can make channel 1 of the phase meter generate a null response to the return signal from target B. By also choosing $f_{PM} = [4(\tau_A - \tau_B)]^{-1}$, one can make channel 1 of the phase meter generate a maximum response to return signal from target A. These choices further cause channel 2 to generate a null response to target A and a maximum response to target B. Thus, the responses to the two targets are separated, making it possible to monitor their displacements separately.

This work was done by Oliver Lay and Serge Dubovitsky of Caltech for **NASA's Jet Propulsion Laboratory**. *Further information is contained in a TSP [see page 1].*

In accordance with Public Law 96-517, the contractor has elected to retain title to this invention. Inquiries concerning rights for its commercial use should be addressed to

Technology Reporting Office
JPL
Mail Stop 249-103
4800 Oak Grove Drive
Pasadena, CA 91109
(818) 354-2240

Refer to NPO-21032, volume and number of this NASA Tech Briefs *issue, and the page number.*

Flexible Carrier-Signal-Tracking Loop for a Transponder

This loop could be programmed for perfect or imperfect integration.

NASA's Jet Propulsion Laboratory, Pasadena, California

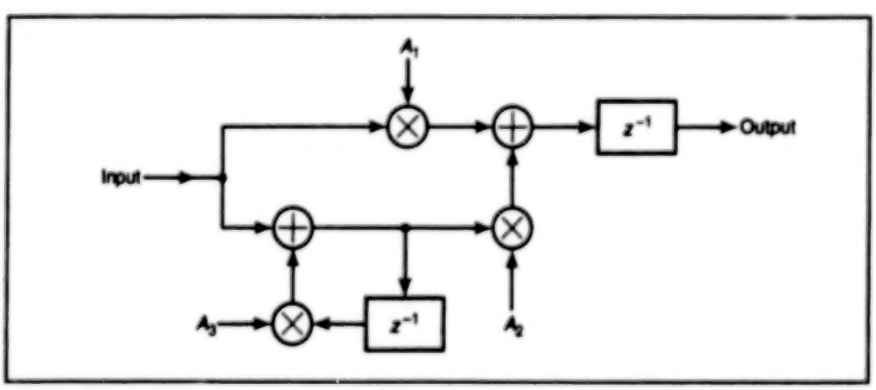

A Loop Filter of this configuration can be made to behave as a perfect or imperfect integrator, depending on the choice of A_1 and A_2 and of a third parameter A_3.

A proposed digital carrier-signal-tracking loop in a radio transponder could be programmed to operate in either a perfect-integration or an imperfect-integration mode. Although originally intended for use in a transponder aboard a spacecraft at a great distance from the Earth, the proposed loop might also be advantageously incorporated into terrestrial communication systems in which it is necessary to track the phases of received carrier signals.

Either imperfect or perfect integration can be advantageous or disadvantageous, depending on state of signal reception. Among specialists in the design of carrier-signal-tracking loops, it is well known that as long as a carrier signal is present, the tracking performance of a loop that contains a perfect integrator is better than that of a loop that contains an imperfect integrator. For example, when the frequency of the received carrier signal is offset from the best-lock frequency by an amount δf, a loop that contains a perfect integrator exhibits zero phase error, whereas a loop that contains an imperfect integrator exhibits a phase error equal to $2\pi\delta f/\alpha K$, where αK is the loop gain. On the other hand, when a loop idles (that is, when the input to the loop consists solely of noise), then for a given loop bandwidth,

the best-lock frequency of the loop drifts less if the integration is imperfect than it does if the integration is perfect.

The proposed loop design would make it possible to choose whichever integration mode — perfect or imperfect — is currently more advantageous. The figure is a block diagram of a loop filter that can implement either mode. The transfer function of the loop can be given by $A_1z^{-1} + A_2/(z - A_3)$, where A_1, A_2, and A_3 are arbitrary parameters and z is the argument of the z transform ($z = e^{sT}$, where T is the sample period of the digital circuitry and s is the complex-frequency variable of the Laplace transform). The transfer function is that of a perfect or imperfect integrator, depending on the choice of A_1, A_2, and A_3.

To obtain a perfect integrator, one must choose

$A_1 = K_1$,

$A_2 = K_2T_U$, and

$A_3 = 1$,

where K_1 and K_2 are parameters that determine the loop performance and T_U is the sample period at the output of the loop error accumulator.

To obtain an imperfect integrator, one must choose

$A_1 = K(T_U - \tau_2)/(T_U - \tau_1)$,

$A_2 = K\{(\tau_2/\tau_1) - [(T_U - \tau_2)/(T_U - \tau_1)]\}$, and

$A_3 = 1 - (T_U/\tau_1)$,

where K is the strong-signal loop gain and τ_1 and τ_2 are the loop time-constant parameters.

It is not necessary to select the parameters A_1 and A_2 with high precision: it suffices to set these parameters within about 1 percent of the values given in the equations above. However, the performance of the loop is quite sensitive to the value of A_3: For an imperfect integrator, A_3 must be set at a value that is less than 1 by a small, precise amount.

This work was done by Jeff Berner, James M. Layland, and Peter Kinman of Caltech for **NASA's Jet Propulsion Laboratory**. *Further information is contained in a TSP [see page 1].*

NPO-20845

Imaging Lidar System Would Map Surface Heights

Potential uses include high-resolution topographical mapping.

NASA's Jet Propulsion Laboratory, Pasadena, California

A proposed optoelectronic system based on imaging-lidar and differential-altimetry techniques would generate data equivalent to a height map of a surface area. Originally conceived for use in determining spatial-frequency characteristics of ocean waves with high temporal resolution, the system could also be used to generate high-resolution topographical maps of terrain or to study the roughness properties of land areas of geological interest.

The system would include a pulsed laser, an electro-optical modulator serving as an electronic shutter, a high-speed digitizer-and-trigger unit, beam splitters, photodetectors, a computer-and-timing-circuit unit, and two charge-coupled-device (CCD) array detectors. The two CCDs must be radiometrically calibrated and co-registered so that corresponding pixels receive light from the same points in the scene.

In operation, the system would illuminate the target surface with a short laser pulse, and both CCDs would image laser light reflected from the target surface. However, the electronic shutter would be activated to truncate the optical return to CCD1 at a time, T_0, after the initial laser-triggering pulse. With knowledge of the time dependence of the laser-pulse intensity, along with the time dependence of the shutter transmittance, it is possible to compute, for each pixel, the round-trip light travel time (T) corresponding to the local surface height.

For this purpose, T_0 is set to some value $\approx T$, such that the shutter would be in the process of closing just as the optical return pulse reached CCD1. It can be seen that nominally T_0 corresponds to the mean height of the target surface.

The mathematical model for computing T (and thus the surface height) would utilize the output signals proportional to the received radiant flux integrated over time. For a given surface point and the corresponding pixel on CCD1, this signal would depend on the round-trip and shutter times and is therefore denoted $S_1(T,T_0)$. On the other hand, CCD2 would integrate the entire return optical pulse, so that the signal from the corresponding pixel of CCD2 would be denoted by $S_2(T,\infty)$.

Both $S_1(T,T_0)$ and $S_2(T,\infty)$ would be influenced by the reflection coefficient of the surface and laser-speckle characteristics. The effect of these unknown factors is eliminated by applying a ratiometric approach:

$$E(T,T_0) = \frac{2S_1(T,T_0) - S_2(T,\infty)}{S_2(T,\infty)}$$

This function increases monotonically with $T_0 - T$, and can be inverted to compute $T[E(S_1,S_2)]$ for each pixel, thus yielding a relief map of the scene with high temporal resolution.

This work was done by Ernesto Rodriguez, Robert T. Menzies, David M. Tratt, and Carlos Esproles of Caltech for **NASA's Jet Propulsion Laboratory**.

NPO-18812

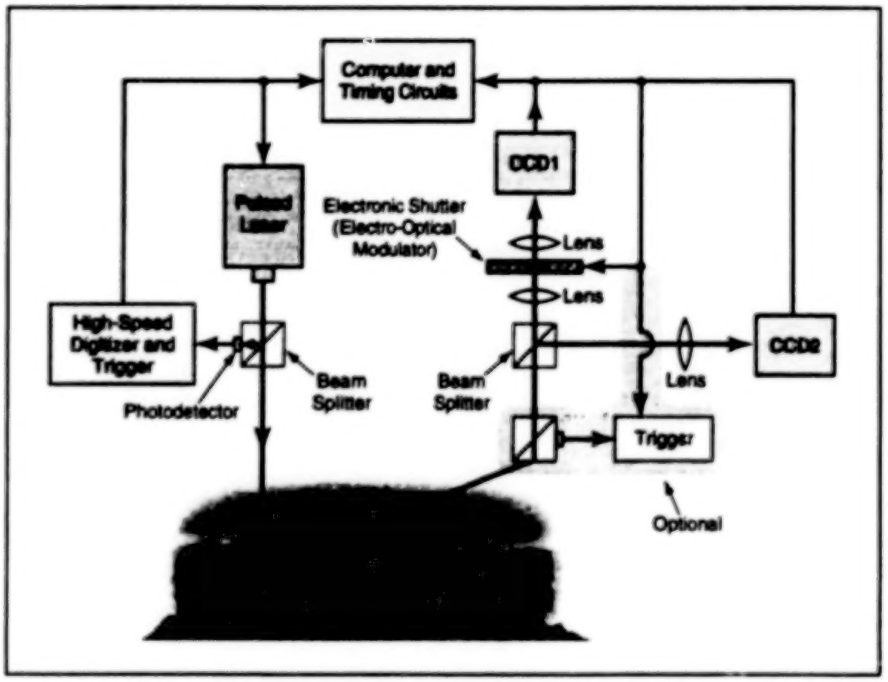

By Suitable Timing of The Electronic Shutter with respect to the laser-trigger pulse, this system would generate different images of the same scene in the two CCDs. One could compute round-trip light-travel times from ratios between light signals integrated by the two CCDs.

BLANK PAGE

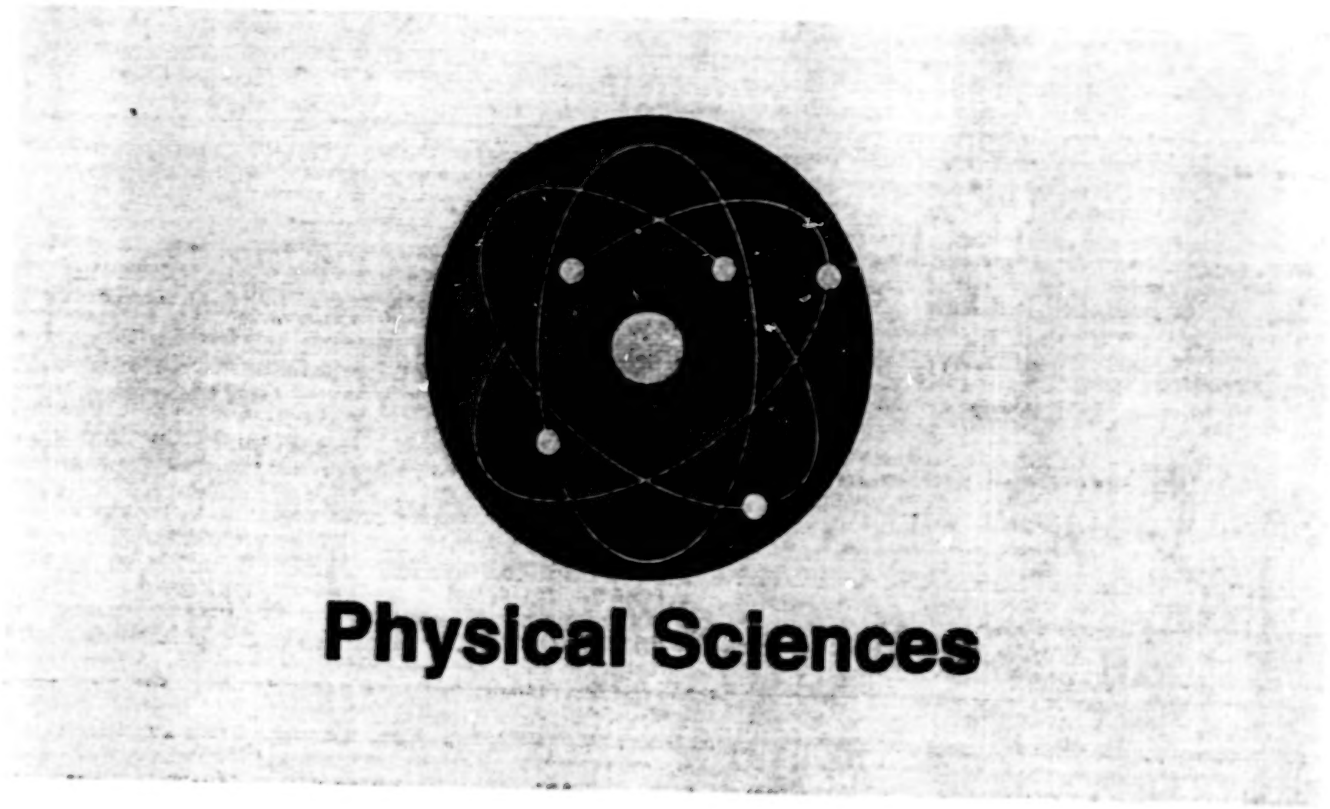

Physical Sciences

Hardware, Techniques, and Processes

Spatially Modulated Prism Interferometer

Advantages include high efficiency over a very broad spectral bandwidth, compactness, mechanical stability, spectral radiometric purity.

NASA's Jet Propulsion Laboratory, Pasadena, California

A spatially modulated prism interferometer (SMPI) has been developed that overcomes the complexities of traditional interferometers and the inherent limitations of diffraction gratings, dispersion prisms, and spectral selection filters. Applications include atmospheric sounding, geologic mapping, *in-situ* mineralogy, oceanography, pollution monitoring, poisonous gas detection, medical spectroscopic imaging, and industrial inspection.

At the heart of the SMPI is the prism triplet shown in Figure 1. Its function is to shear the input beam into two mutually coherent output beams with chief rays that are parallel to the optical axis. A Fourier optical system, shown in Figure 2, collimates the two beams, tilts them, and then recombines them at a pupil plane. The tilted wavefronts generate a spatially modulated interference pattern that is recorded as an interferogram by a detector array. If the Fourier optical system is made anamorphic, then a line image is formed in a direction orthogonal to the series of interferograms. Interferometers with a 25° image field have been designed.

Because the SMPI generates instantaneous interferograms at a pupil plane, it benefits from the following attributes:

- **Field-Widened:** The entrance slit can be widened to any width to increase the signal flux without affecting the spectral resolution. This gives it a significant advantage over grating and prism spectrometers, which must trade throughput for spectral resolution. Image plane interferometers suffer a similar fate because their modulation efficiency degrades in proportion to the slit width and fringe frequency, a phenomenon known as self-apodization.
- **Broadband Efficiency:** As shown in Figure 1, the SMPI efficiency is nearly constant with wavelength. In contradistinction, the efficiency of a grating spectrometer is high only at the blaze wavelength, and then it diminishes rapidly. The SMPI has double the efficiency of the Michelson, Sagnac, and Wollaston prism interferometers because it utilizes all (instead of half) the incident light.
- **No Stray Light Induced Spectral Errors:** Stray light in the SMPI increases the noise floor but does not necessarily contribute to an erroneous spectral signal. In filter, prism, and grating spectrometers, stray light is indistinguishable from spectral signals and introduces large radiometric errors. Gratings are particularly troublesome because they behave like badly scratched mirrors. The edge of each groove, even when perfectly fabricated, scatters the incident white light directly across the spectrum.
- **Radiometric Purity:** When the detector array is at a pupil plane the radiance contributions from the various objects in the field are uniformly distributed across the pixels in the array. A pupil plane interferometer has the additional benefit of distributing all the colors of the spectrum uniformly across all the pixels of the array. This simplifies calibration and eliminates the radiometric errors that are routinely generated in image-plane spectrometers and filters when high radiance objects are lost in the dead zones between pixels. Responsivity variations across the active regions of pixels also contribute to radiometric errors in image-plane spectrometers, which is why they should not be used in science applications that require high spectral radiometric accuracy.

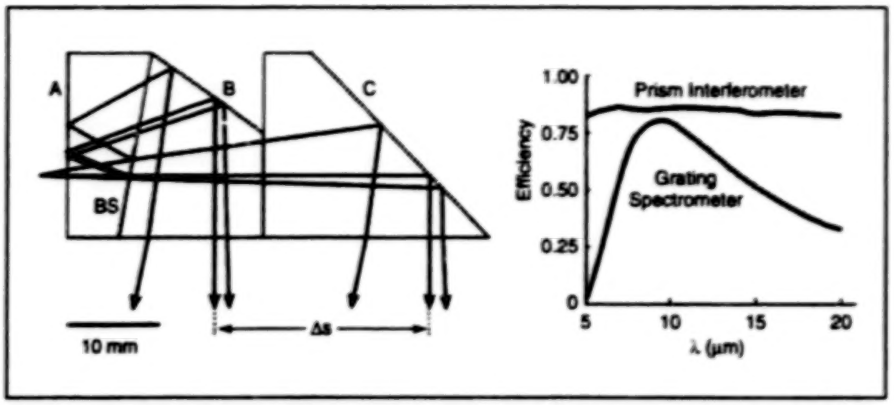

Figure 1. The Beam-Shearing Prism Triplet is made from a single-crystal material to maintain the same optical path length for both beams. Its unique design enables the spatially modulated prism interferometer to have double the efficiency of conventional interferometers and a much broader spectral pass-band than grating spectrometers.

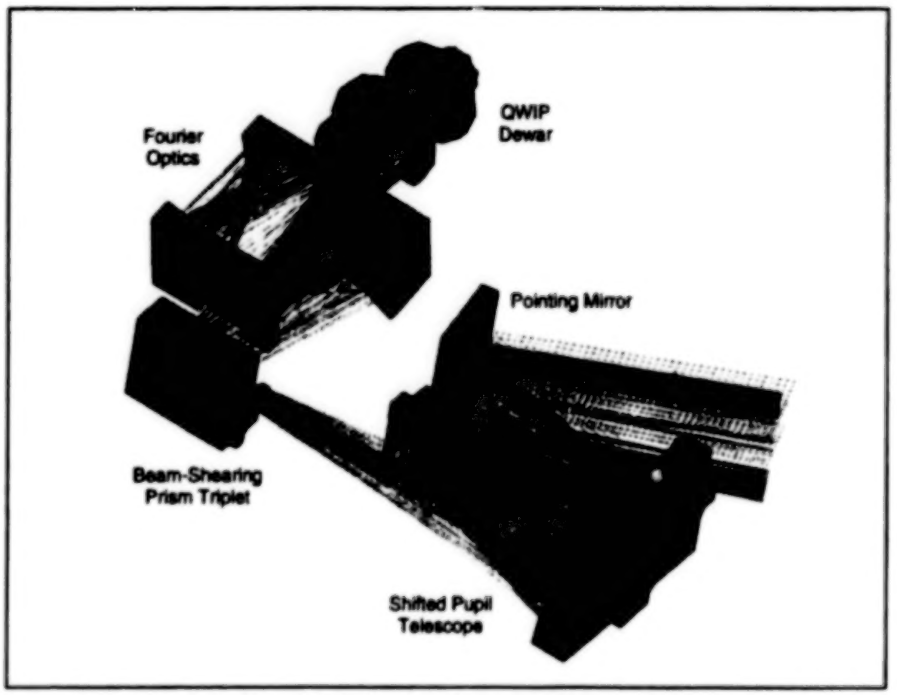

Figure 2. This **Spatially Modulate Prism Interferometer** design has a spectral resolution of 1.2 cm^{-1}. It uses a shifted pupil telescope to double the spectral resolution and toroidal mirrors in the Fourier optics to maximize the spatial resolution.

- **Single Instrument Line Shape Function:** There are no diffraction effects at a pupil plane, so the SMPI can be designed to have a single line shape for all colors and field positions. This greatly simplifies calibration and spectral retrievals in comparison to image-plane gratings, dispersive prisms, and filters. The line shape generated by these devices broadens with wavelength-dependent diffraction and changes with the aberration-dependent point-spread function.
- **Instantaneous Interferogram:** The entire interferogram is recorded instantaneously across the detector array, which eliminates recording errors. Scanning interferometers and filters that require the movement of the observational platform or an optical component are prone to irrecoverable spectral errors when the platform motion is not perfectly rectilinear or the scene changes during the scan period.
- **Mechanical Stability:** Unlike Michelson interferometers, the SMPI is relatively insensitive to mechanical shock, focal plane jitter, and misalignment because there are no moving parts, and because the two beams converging on the detector array are collimated. The collimation attribute relaxes the focal plane axial position tolerance: a 1-mm axial shift generates less than 0.5-percent change in the spectral line width at 5 cm^{-1} resolution, and no change in the spectral line position. Since a typical axial position tolerance is 10 μm and the typical axial vibration amplitude of an active cooler is 1 μm, the detector array can be mounted directly onto the cold finger without concern for vibration-induced spectral errors. This significantly reduces the cooling power requirements and the complexity of the thermal-mechanical focal-plane mount.

The SMPI incorporates several important optical design characteristics that enable it to achieve high spectral resolution and high efficiency in a compact form. The telescope is designed with a shifted pupil so that the chief ray strikes the edge rather than the middle of the detector array. This shifts the zero path difference point to one side of the array and effectively doubles the maximum possible optical-path difference and spectral resolution without requiring a doubling of the pupil width.

The beam-shearing prism is designed so that the beam splitter (BS) coating on prism A is tilted less than 10° to the input beam. This prevents total internal reflection at the airgap between prisms A and B, and it eliminates the need for an oil or adhesive to fill the gap. Adhesives have strong absorption features in the thermal infrared, so their omission is desirable.

The prism configuration is governed by a requirement to maintain the same optical path length for two light beams whose chief rays must emerge parallel to each other and perpendicular to a flat output surface. When the entrance and exit surfaces are perpendicular to the chief rays, then astigmatism and dispersion are eliminated. Astigmatism reduces the spectral resolution of the interferometer, and dispersion changes the instrument line shape as a function of wavelength.

The prism is designed for minimum volume and maximum beam shear. The beam shear distance, ΔS, is proportional to the spectral resolution. A thumb-sized beam-shearing prism with a 60-mm focal length Fourier lens can achieve a spectral resolution of 1 cm^{-1}. This is a factor of 40 reduction in volume with respect to an equivalent Sagnac interferometer. Likewise, a 0.5 cm^{-1} prism interferometer can improve by a factor of two the NEΔT of the Atmospheric InfraRed Sounder (AIRS) and reduce its volume by a factor of 25. AIRS is a pupil plane grating spectrometer.

The high-resolution performance of the SMPI is due in no small part to the recent advances in large format, GaAs based Quantum Well Infrared Photoconductor (QWIP) detector arrays. The SMPI requires a large array of pixels with high pixel operability and uniform responsivity, which are two unique characteristics of the QWIP arrays being developed at JPL (see Tech Briefs Vol. 24, No. 5, p. 26a-30a). The QWIP arrays also have low 1/f noise, which increases the calibration stability of the detector array and of the interferometer.

This work was done by Francis Reininger of Caltech for ***NASA's Jet Propulsion Laboratory****. Further information is contained in a TSP [see page 1].*

In accordance with Public Law 96-517, the contractor has elected to retain title to this invention. Inquiries concerning rights for its commercial use should be addressed to

Technology Reporting Office
JPL
Mail Stop 249-103
4800 Oak Grove Drive
Pasadena, CA 91109
(818) 354-2240

Refer to NPO-20647, volume and number of this NASA Tech Briefs *issue, and the page number.*

Snapshot SEM Imaging of Moving MEMS Structures

The principle of stroboscopy would be extended to scanning electron microscopy.

NASA's Jet Propulsion Laboratory, Pasadena, California

A stroboscopic scanning electron microscope (SEM) has been proposed as a means of generating still or slow-motion pictures of moving structures in microelectromechanical systems (MEMS). Such imaging is used in characterizing the dynamics of MEMS; characterization of the dynamics is a critical component of the MEMS development cycle.

Conventional strobed-illumination microscopy with visible or infrared light provides adequate temporal resolution but insufficient spatial resolution for measuring subwavelength motions in the main plane of a typical MEMS. A conventional SEM provides adequate spatial resolution, but is inadequate for resolving motions at frequencies greater than several tens of hertz because the illuminating electron beam is continuous. The proposed stroboscopic SEM would offer both the spatial resolution of a conventional SEM and the temporal resolution of conventional optical stroboscopy, making it possible to form crisp images of moving (e.g., vibrating) MEMS structures.

According to the proposal, a conventional SEM would be augmented with an electronic beam blanker that would be operated in coordination with a signal generator. The output of the signal generator would control the vibrational excitation of a MEMS device mounted in the SEM (see figure).

In one mode of operation, the blanking-pulse-repetition frequency would be set equal to the frequency of vibration, so that the resulting SEM image would "freeze" the motion at some phase in the

vibration cycle. The phase could be varied by adjusting the phase offset between the vibration-waveform and blanking-pulse generators. In another mode of operation, the blanking-pulse-repetition frequency would be made to differ slightly (no more than a few hertz) from the vibration frequency, yielding a sequence of images at slightly different phases (in other words, a slow-motion picture). Freeze-motion images taken at different phases could be used to quantify the shape of a vibrational mode at the frequency of excitation, while slow-motion pictures could be used to obtain qualitative understanding of the motion.

This work was done by Kirill Shcheglov and Russell Lawton of Caltech for **NASA's Jet Propulsion Laboratory**. *Further information is contained in a TSP [see page 1].*
NPO-21056

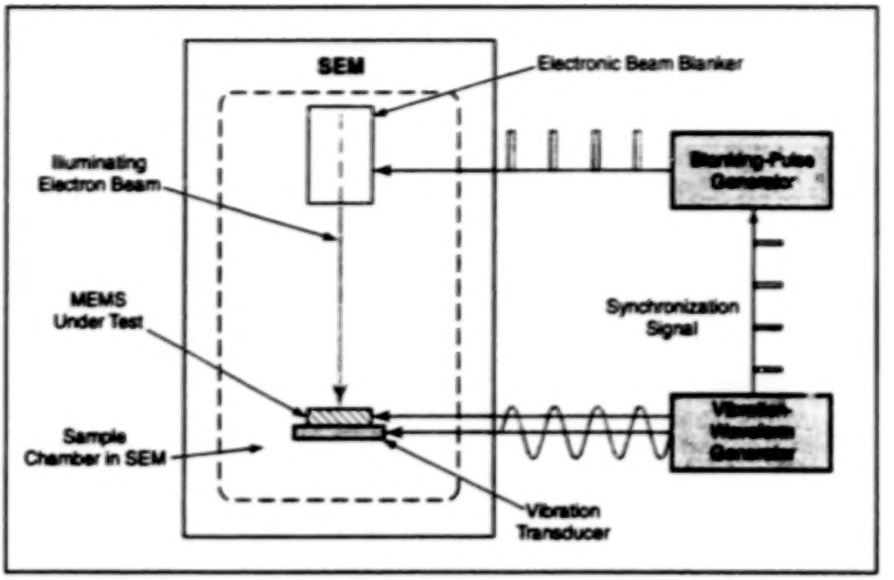

Vibrational Excitation and Blanking Pulses would be synchronized or nearly synchronized to obtain snapshots or slow-motion pictures, respectively, of the vibrating MEMS.

Surface Gratings for Optical Coupling With Microspheres

Far-field coupling offers advantages over near-field coupling.

NASA's Jet Propulsion Laboratory, Pasadena, California

A diffraction grating consisting of a periodic gradient in the index of refraction of a thin surface layer has been shown to be effective as a means of far-field coupling of monochromatic light into or out of the "whispering-gallery" electromagnetic modes of a transparent microsphere. This far-field coupling can be an alternative to the near-field (evanescent-wave) coupling afforded by prism- and fiber-optic couplers described in NPO-20619 on page 23 of this issue. Far-field coupling is preferable to near-field coupling in applications in which there are requirements for undisturbed access to the entire surfaces of microspheres. Examples of such applications include (1) a proposed atomic cavity in which cold atoms would orbit in a toroidal trap around a microsphere and (2) a photonic quantum logic gate based on coupling between a high-Q (where Q is the resonance quality factor) microsphere and trapped individual resonant ions.

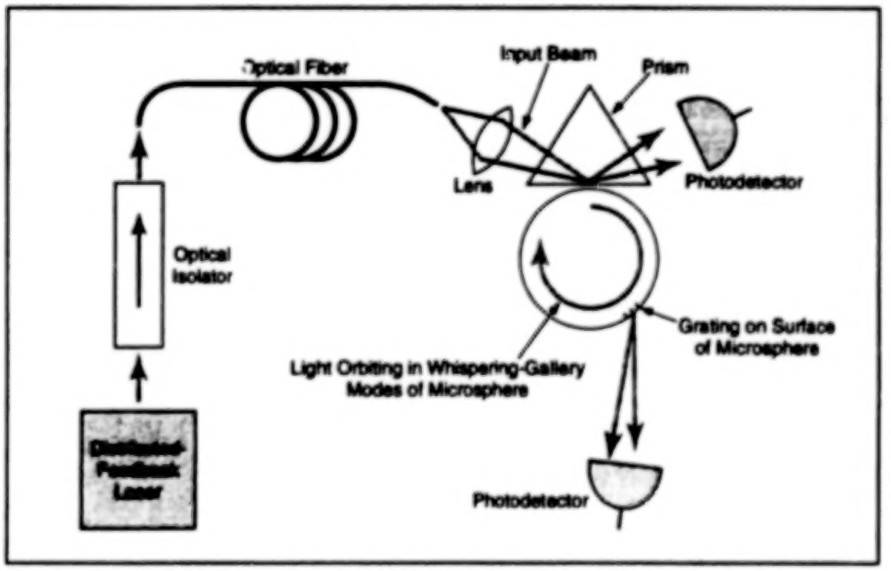

Figure 1. Laser Light Was Coupled into the microsphere via the prism, then coupled out via the grating. The output beam was oriented at an angle of about 40° with the surface, with 80 percent of its power concentrated in a single lobe with a divergence of 11°.

In preparation for experiments to demonstrate this concept, fused silica microspheres with a diameter of about 180 μm were fabricated, then coated with layers of molten germanium-doped glass powder 3 to 5 μm thick. The purpose served by the germanium doping was to increase the photosensitivity of the surface layers for the grating-fabrication step described next. An index-of-refraction grating was formed in the surface layer of each microsphere by exposing the layer to ultraviolet light (wavelength = 244 nm) from a frequency-doubled argon laser. The laser beam power was 40 mW, the exposure time was 5 to 10 minutes, and the expected index modulation was (1 to 3) × 10^{-4}. The spatial period and length of the grating were ≈2 μm and ≈15 μm, respectively. The spatial period was chosen to provide first-order phase matching between a whispering-gallery mode of the microsphere and a free-space beam oriented at ≈45° to the surface of the microsphere.

Figure 1 schematically depicts the experimental setup used to demonstrate the grating-based coupling scheme. Laser light at a wavelength of ≈1,550 nm was coupled into the whispering-gallery modes of a microsphere by a standard prism coupler, then coupled out of the microsphere by the grating. The laser was gradually tuned over a frequency range that included some whispering-gallery-mode resonances. The resulting measurements (see Figure 2) showed

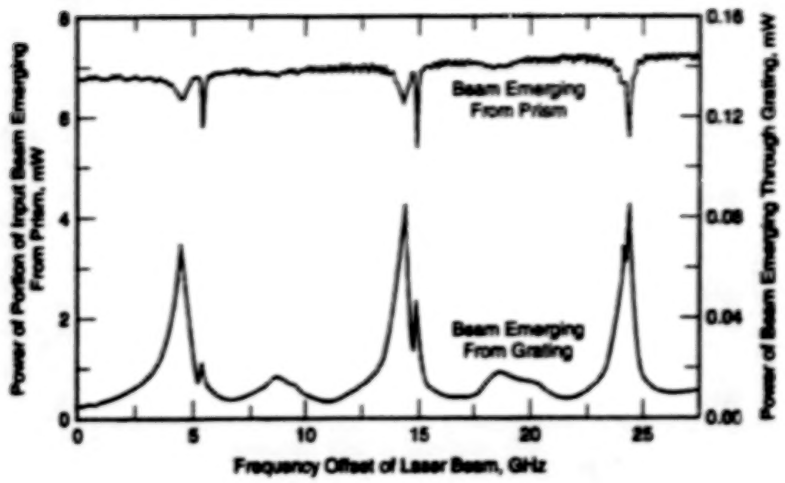

Figure 2. Whispering-Gallery-Mode Resonances are readily apparent in the spectra measured in the setup of Figure 1.

that at the resonances, some light was depleted from the input beam and there were corresponding increases in the amount of light emitted from the microsphere through the surface grating.

From the measurement data, the maximum grating coupling efficiency was calculated to be 14 percent. The grating loaded the resonance sufficiently to decrease the Q of the microsphere to a value in the range of $(0.2 \text{ to } 2) \times 10^6$. [The initial Q (without the grating) was 1.2×10^8.] Higher Q could be obtained by reducing the strength of the grating. Efficiency of coupling could be increased by optimizing the exposure to ultraviolet light, improving the grating profile, and minimizing scattering losses. Parasitic coupling to low-Q higher-order modes in the microsphere could be prevented by decreasing the diameter of the microsphere.

This work was done by Vladimir Iltchenko and Lute Maleki of Caltech for **NASA's Jet Propulsion Laboratory.** *Further information is contained in a TSP [see page 1].*

In accordance with Public Law 96-517, the contractor has elected to retain title to this invention. Inquiries concerning rights for its commercial use should be addressed to

Technology Reporting Office
JPL
Mail Stop 249-103
4800 Oak Grove Drive
Pasadena, CA 91109
(818) 354-2240

Refer to NPO-20618, volume and number of this NASA Tech Briefs *issue, and the page number.*

Optics for Compact, High-Performance Imaging Spectrometers

An off-axis, telecentric telescope/camera is combined with convex diffraction grating spectrometers.

NASA's Jet Propulsion Laboratory, Pasadena, California

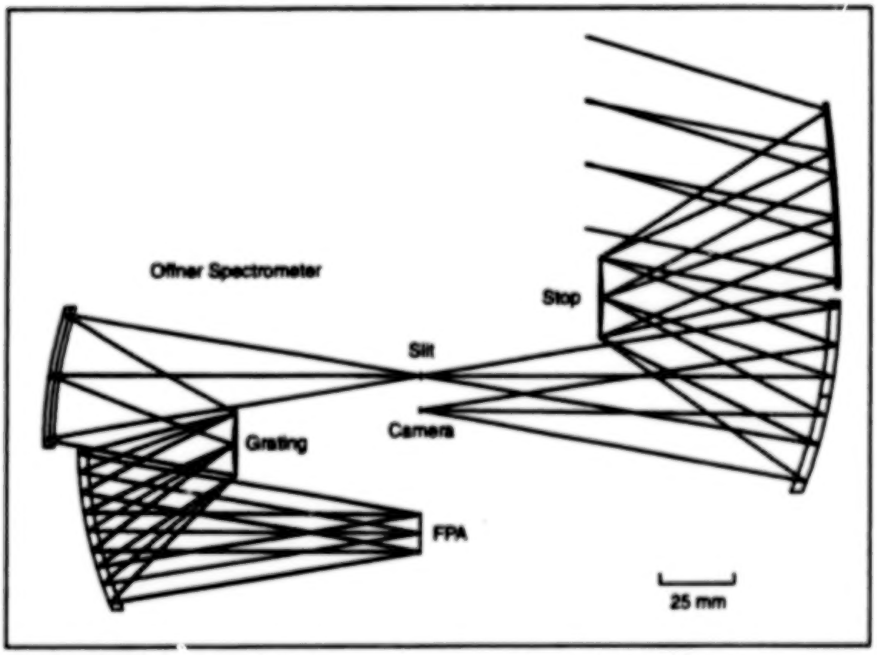

This Imaging Spectrometer/Camera uses a convex grating in a lateral Offner configuration to reduce distortion to less than 1 percent across a 12-mm spectrum with a 16-mm image.

Several high-fidelity imaging spectrometers have been designed with convex diffraction gratings for wavelengths ranging from the ultraviolet to the thermal infrared. All the designs are telecentric and can be combined with a flat-field, three-mirror anastigmatic telescope that also functions as a panchromatic camera.

The spectrometers are derivatives of an elegant relay disclosed by Offner in the early 1970's. The original "Offner relay" was a mask aligner consisting of two concentric spherical mirrors for projecting a telecentric image of a mask onto a semiconductor wafer. A few years later Thevenon suggested replacing the convex secondary mirror of the relay with a diffraction grating to form an imaging spectrometer.

In 1992, an Italian firm decided to act on Thevenon's suggestion and developed the first compact Offner imaging spectrometer for the Cassini mission to Saturn. Dubbed the "VIMS-V", the prototype was delivered to the Jet Propulsion Laboratory (JPL) for integration into the "Visible Infrared Mapping Spectrometer." The grating for the VIMS-V was manufactured by a German company using holographic recording and ion-beam milling. The gratings can also be fabricated using electron-beam lithography.

The Offner spectrometer was initially developed to overcome the inherent limitations of another popular concentric spectrometer invented by Dyson in the late 1950's. The Dyson uses a concave grating and controls optical aberrations with a thick plano-convex lens placed immedi-

ately in front of the slit-detector plane. Unfortunately a lens in this position backscatters the input white light directly onto the focal plane array (FPA), and it does not leave space for a cold stop. Without a cold stop the entire spectrometer must be cooled to the FPA temperature, thereby increasing the low temperature cooling load by a factor of 10 or more.

A cold Dyson spectrometer would also be sensitive to misalignment because its grating reflects the chief rays at large angles to the optical axis before they can be made telecentric by the lens. Hence, a small shift in the position of the lens distorts the image and the spectrum. For example, a shift within a typical position tolerance of 10 μm generates 8 percent distortion at the edge of a spectrum only 5 mm long.

An acceptable *uncalibrated* distortion limit is 1 percent of a pixel, which is easily controlled in the Offner when the spectrum is confined to a narrow, annular zone less than a few millimeters wide. Two examples of miniature Offner designs with less than 10 nm distortion (0.1 percent of a pixel along a 16 mm image) are listed at *http://focus.software.com/file-exchange/index.html*.

Distortion increases as the cube of the spectral length, so it becomes increasingly difficult to maintain performance across large-area FPAs. The new designs use several variations of Offner configurations to maintain high performance across large areas. In the design shown in the figure, the image is 16 mm long and the spectrum is 12 mm long, yet the spectral distortion is less than 1 percent of a pixel. This is accomplished by tilting the two relay mirrors of a lateral Offner configuration (the grating and FPA are displaced laterally from the slit line).

In another design the image is 12 mm long and the spectrum is 16 mm long, so the Offner is put into a vertical configuration (the grating and FPA are displaced vertically above the slit line). A single, aspheric relay mirror helps control optical aberrations. The vertical configuration enables the grating to be divided into two sections that are blazed for positive and negative diffraction orders. Each section is optimized for its own FPA spectral passband and resolution. This technique is used in an imaging spectrometer being developed for the comet rendezvous mission *Rosetta*. The spectrometer can cover the 0.25 – 5 μm spectral band without the need for a dichroic beam splitter. Dichroic beam splitters limit the spectral passband considerably, especially when the passband extends from the ultraviolet to the infrared.

This work was done by Francis Reininger of Caltech for **NASA's Jet Propulsion Laboratory**. *Further information is contained in a TSP [see page 1].*

In accordance with Public Law 96-517, the contractor has elected to retain title to this invention. Inquiries concerning rights for its commercial use should be addressed to

Technology Reporting Office
JPL
Mail Stop 249-103
4800 Oak Grove Drive
Pasadena, CA 91109
(818) 354-2240

Refer to NPO-20239, volume and number of this NASA Tech Briefs *issue, and the page number.*

Simple Fiber-Optic Coupling for Microsphere Resonators

The "pigtailed" ultra-high-Q microcavities make a novel building block for fiber-optic systems.

NASA's Jet Propulsion Laboratory, Pasadena, California

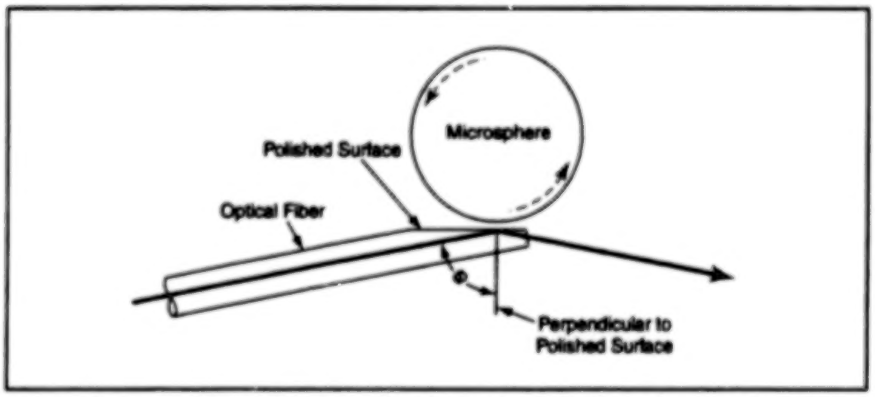

Figure 1. Evanescent-Wave Coupling takes place in the gap between the microsphere and the angle-polished surface on optical fiber. The angle (Φ) is chosen to match phases of waves propagating in the optical fiber and the microsphere.

Simple fiber-optic couplers have been devised for use in coupling light into and out of the "whispering-gallery" electromagnetic modes of transparent microspheres. The need for this type of coupling arises in conjunction with the use of transparent microspheres as compact, high-*Q* (where *Q* is the resonance quality factor) resonators, delay lines for optoelectronic oscillators (including microlasers), and narrow-band-pass filters.

In the whispering-gallery modes of a transparent microsphere, light orbits inside the sphere, where it is confined by total internal reflection. The high degree of confinement results in high *Q* (up to about 10^{10} in the absence of loading). To couple light into or out of the microsphere, it is necessary to utilize overlapping of (1) the evanescent field of the whispering-gallery modes with (2) the evanescent field of a phase-matched optical waveguide or of an optimized total-internal-reflection spot in a prism or similar component. Heretofore, such coupling has been implemented, variously, by use of tapered optical fibers, side-polished optical fibers, or prisms, all of which entail disadvantages:

- Tapered optical fibers are fragile, bulky, and difficult to fabricate.
- Side-polished optical fibers offer low efficiency.

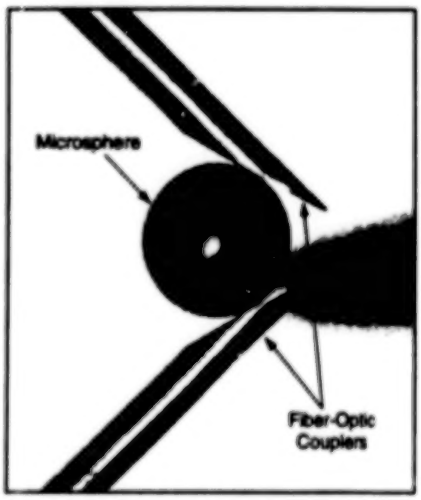

Figure 2. Input and Output Fiber-Optic Couplers were placed in proximity to a silica microsphere of 203-μm radius. The total fiber-to-fiber transmission loss at resonance was 6.3 dB (~25 percent of the input light passing through the cavity), with the quality-factor ~1 × 10^8 at 1.55 μm.

- Prisms are bulky and require collimation and focusing optics to work with optical fibers.

In contrast, the present fiber-optic couplers are simple, compact, and relatively inexpensive. A coupler of this type is essentially a hybrid of a waveguide and a prism coupler, and provides direct coupling with high-Q whispering-gallery modes. The coupler is fabricated by cleaving and polishing the tip of a single-mode optical fiber at an angle to form a microscopic coupling prism integral with the fiber. The cleaved and polished surface lies at a small angle ($\pi/2-\Phi$) with the longitudinal axis of the fiber (see Figure 1). The angle is chosen to secure matching of phases of the waveguide and whispering-gallery modes; by Snell's law, the angle is given by $\Phi = \arcsin(n_{sphere}/n_{fiber})$, where n_{sphere} is the effective index of refraction for the whispering-gallery modes propagating around the sphere in closed circumferential orbits and n_{fiber} is the effective index of refraction for the guided wave in the truncated region of the fiber-optic core.

In the absence of a nearby microsphere, light propagating along the fiber is totally internally reflected at the angled surface and then escapes through the end face of the fiber. If a microsphere is placed near the angled surface and within the evanescent field of the fiber-optic core, then there is an efficient exchange of energy in resonance between the waveguide mode of the fiber and a whispering-gallery mode of the sphere. Inasmuch as the angle-cut area of the fiber coincides, to a close approximation, with the area of overlap of the evanescent fields, the present coupler is functionally equivalent to a prism coupler, without need for collimation and focusing optics.

Figure 2 depicts an experimental setup that was used for testing this coupling method. Efficiency of input and output coupling was measured by simultaneous monitoring of the intensity of the light escaping from the end of the input optical fiber and the power transmitted to the output optical fiber. In the experiments, the gaps between the microsphere and the angled coupling faces of the optical fibers were adjusted to optimize contrast of resonances in input coupling and maximize the power transmitted to the output optical fiber.

The experiments showed that this method of coupling works well, allowing to couple, at resonance, up to 60 percent of the light from the input fiber into the microsphere. The total fiber-to-fiber insertion loss at resonance was about 6 dB, with the quality-factor ~10^8 at the wavelength 1.55 μm.

This work was done by Lute Maleki, Vladimir Ilchenko, and Steve Yao of Caltech for **NASA's Jet Propulsion Laboratory**. *Further information is contained in a TSP (see page 1).*
NPO-20619

Determining Particle Sizes From Scattered-Photon Statistics

A relatively simple, compact apparatus quickly yields approximate results.

John H. Glenn Research Center, Cleveland, Ohio

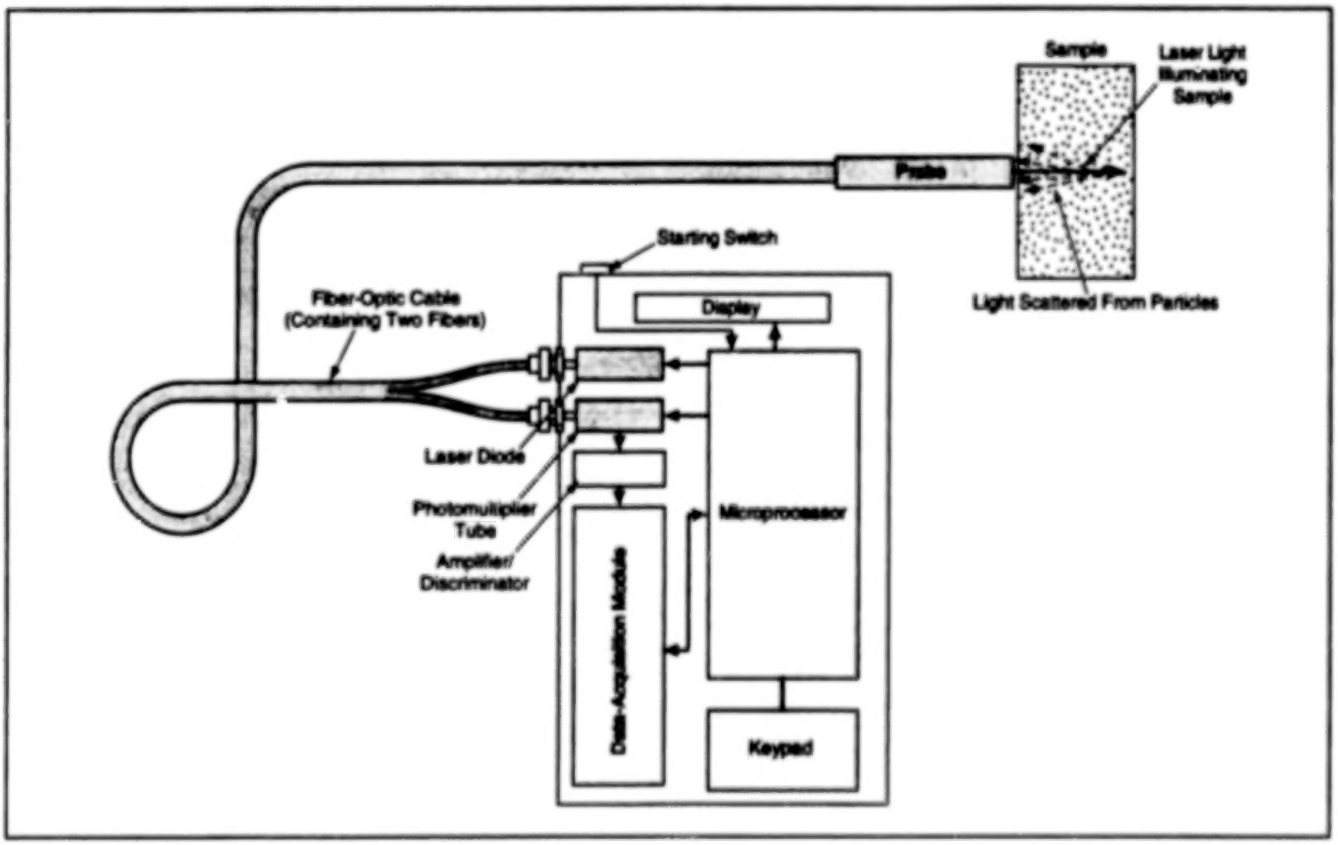

A Portable Optoelectronic Instrument illuminates a liquid sample with coherent light, counts photons scattered from particles suspended in the liquid, and computes the average size of the particles from photon-counting statistics.

A method of determining sizes of particles suspended in liquids and engaging in Brownian motion involves statistical analysis of counts of photons of laser light scattered by the particles. The method can be implemented by a compact, portable apparatus that can be used, for example, in monitoring of colloidal suspensions, characterization of suspended protein molecules, and the like.

In the prior state-of-the-art light-scattering method for determining particle sizes, one performs a digital correlation followed by an ill-conditioned inversion to obtain a particle-size distribution. The disadvantage of the prior method is that the equipment (especially the computer needed to perform the correlation) is expensive and usually too large and complex to be portable, and the measurements and computations take a few minutes. In the present method, one does not obtain a particle-size distribution; on the other hand, one can estimate the average size of light-scattering particles in a sample after a measurement and computation time of a few seconds.

This method is an instance of photon-correlation spectroscopy (PCS). As such, it is closely related to dynamic-light-scattering (DLS) methods, which are based on the concept of extracting information on the sizes and motions of light-scattering particles from the spatial and temporal dependence of the loss of coherence of scattered laser light. The differences between DLS and PCS arise from the fact that in DLS, one operates photodetectors and associated signal-processing circuits in a photocurrent-measuring regime, whereas in PCS, one operates in a photon-counting regime.

The theoretical basis of the present method is not simple; the mathematical derivation would greatly exceed the space available for this article. However, the underlying theory yields an important benefit: in comparison with other light-scattering methods for measuring particle sizes, this method is relatively simple in practice and involves much less computation.

A typical apparatus used in the present method (see figure) includes a laser diode as the source of light. A monomode optical fiber delivers the light to a probe that is placed in contact with, or proximity to, a sample. A short length of multimode optical fiber with a gradient in the index of refraction is fusion-spliced to the end of the monomode fiber to provide focussing of the light delivered by the probe to the sample. The light emerging from the probe illuminates a small volume in the sample. A portion of the light back-scattered from particles in the sample is collected by the probe, and a second optical fiber couples this collected light to a photomultiplier tube. Under control by a microprocessor, the photomultiplier output is processed by an amplifier/discriminator to obtain equal-amplitude voltage pulses at times that correspond to the times of arrival of the collected scattered photons and then processed by a data-acquisition module.

The aforementioned lengthy mathematical derivation elucidates the relationships among temporal coherence of scattered light, photon-counting statistics, and average particle size. One of the results of the derivation is that the temporal coherence of the scattered light depends on both the integration time and the particle diameter. Consequently, it is possible to estimate the average particle size from the degrees of coherence of the photon counts accumulated during two different integration times — T and KT. The values of T and K are chosen to cover a reasonable range of particle sizes by use of the fastest available electronic circuitry. For example, the choice of T = 200 ns and K = 25 makes it possible to estimate diameters from 5 to 3,000 nm.

This work was done by Harbans S. Dhadwal and Kwang I. Suh of the State University of New York for **Glenn Research Center.** *Further information is contained in a TSP [see page 1].*

Inquiries concerning rights for the commercial use of this invention should be addressed to NASA Glenn Research Center, Commercial Technology Office, Attn: Steve Fedor, Mail Stop 4–8, 21000 Brookpark Road, Cleveland, Ohio 44135. Refer to LEW-16706.

A Mass-Spectrometer System for Detecting Gas Leaks

This versatile, expandable system can be controlled from a safe remote location.

John F. Kennedy Space Center, Florida

The Hydrogen Umbilical Mass Spectrometer (HUMS) consists of an integrated sample delivery system, a commercial mass-spectrometer-based gas analyzer, and a set of calibration gas mixtures traceable to NIST (National Institute for Standards and Technology). The system, except for the calibration gas mixtures and the remote operator display, fits into a standard 24-in. wide, 6-ft high, 36-in. deep (0.61 by 1.83 by 0.91 m, respectively) equipment rack and is powered by 120-Vac, 30-A, 60-Hz source. It was designed to perform leak detection and measurement of cryogenic propellants (oxygen and hydrogen) from a remote location during shuttle-launch countdown. It is used specifically to sample the background gas surrounding the 17-in. (0.43-m) Orbiter-ET disconnect, looking for leakage of gaseous hydrogen. The capability to monitor shuttle purge gases and cryogenic hydrogen fill and drain line T-0 disconnect helium purge gas is incorporated into the shuttle installation on each Mobile Launch Platform (MLP).

HUMS was designed to switch rapidly between background gases (helium, nitrogen, or air) during normal operation. The operator has the ability to remotely select one of eight sample lines and between any of six calibration gas mixtures. It can measure from 0 to 100 percent hydrogen, helium, or nitrogen; 0 to 25 percent oxygen; and 0 to 1 percent argon, in any combination in either a helium, nitrogen, or air background. It has an internal cycle mode, added after installation, to cycle between various pre-set sample and calibration gas lines on a continuous basis, if desired.

Operational features include the ability to update the reading for background of each gas in the mixture, thereby avoiding performance of a complete recalibration during operation. This saves a considerable amount of time. The zero gas for the background of interest must be monitored for a couple of minutes to allow the system to stabilize and a reading taken. Only the zero coefficient in the calibration equation for the background of interest is updated. Switching between backgrounds requires only changing to the new background and updating the zero reading for each species. This flexibility is critical when testing in an environment where samples are taken from helium, nitrogen, and air during the test. After testing is complete, a sequence of readings in each background, consisting of zero, test, and span gas mixtures, in that order, provides post-

test verification that the system performance remained unchanged since the initial calibration was performed, pre-test.

Selection of calibration gas mixture concentrations was critical to remote verification of performance. Three concentrations of each gas are included, each in backgrounds of helium and nitrogen. This calibration/verification technique was developed after installation of the Hazardous Gas Detection System (HGDS) in 1979 and is based on experience gained during operation of that system. The performance of the COTS multigas, multicollector magnetic sector analyzer is slightly dependent on background gas, whether helium or nitrogen dominates the mixture. Independent calibration curves are used, depending whether the unknown sample is drawn from either a helium or nitrogen/air background.

During the calibration process, linear calibration curves are generated for each gas in the mixture (hydrogen, helium, nitrogen, oxygen, argon), based on pure background (helium or nitrogen) and a span gas (1 to 10 percent of each gas, in each background). An independent test gas, containing mixtures approximating red-line levels (where action is to be taken, based on readings of the sample) is used to both verify a good calibration (test gas reading lies on the line generated by zero and span, for each species) and to compare directly with the unknown sample, if necessary, to remove uncertainty in reading the unknown mixture. The choice of calibration gases allows differentiation of leak sources of cryogenic oxygen from oxygen contained in air. The operator has the ability to measure the ratio of oxygen to argon (~20), indicative of air intruding into the purge gas. Cryogenic oxygen contains no argon.

The design of HUMS achieved two goals. The first was to provide a permanently installed replacement for the Interim-HUMS (I-HUMS), a system designed and built over a weekend (in part to support nearly simultaneous STS-35, STS-38 launch attempts) to be portable between shuttle MLPs. I-HUMS replaced the one-time installation of the Turbo Mass Spectrometer (TMS) developed for launch of STS-26R (first shuttle launch after 51-L). TMS was designed to verify the performance of the 17-in. (0.43-m) Hydrogen Orbiter-ET Disconnect during hydrogen fill and drain operations, prior to shuttle launch. TMS demonstrated the ability of a high-vacuum turbo-molecular pump to operate and survive in a high vibration environment.

Use of a turbo-molecular pump replaced the need for ion pumps to achieve high vacuum for the mass-spectrometer-based gas analyzer. Ion pumps are unable to pump high concentrations of helium, restricting earlier versions of mass spectrometers to sampling in backgrounds of either nitrogen or air. The HUMS data acquisition and control system was designed to match the standard CORE interface planned to replace the Shuttle Launch Processing System (LPS), but retrofitted to interface with a standard LPS "XCard" when the CORE concept was abandoned during HUMS.

This work was done by Greg Brazzle, Barry Davis, and Frederick Adams of **Kennedy Space Center**; *Guy Naylor, Francisco Lorenzo-Luaces, Charles H. Curley, Richard J. Hiltz, Terry D. Greenfield, David P. Floyd, Curtis M. Lampkin, Donald Young, Gary N. McKinney, and Don Greene of Lockheed-Martin; and David R. Wedekind, Larry Lingvay, and Andrew P. Schwalb formerly of I-NET. For further information, see TSP's [page 1].*
KSC-12109/06

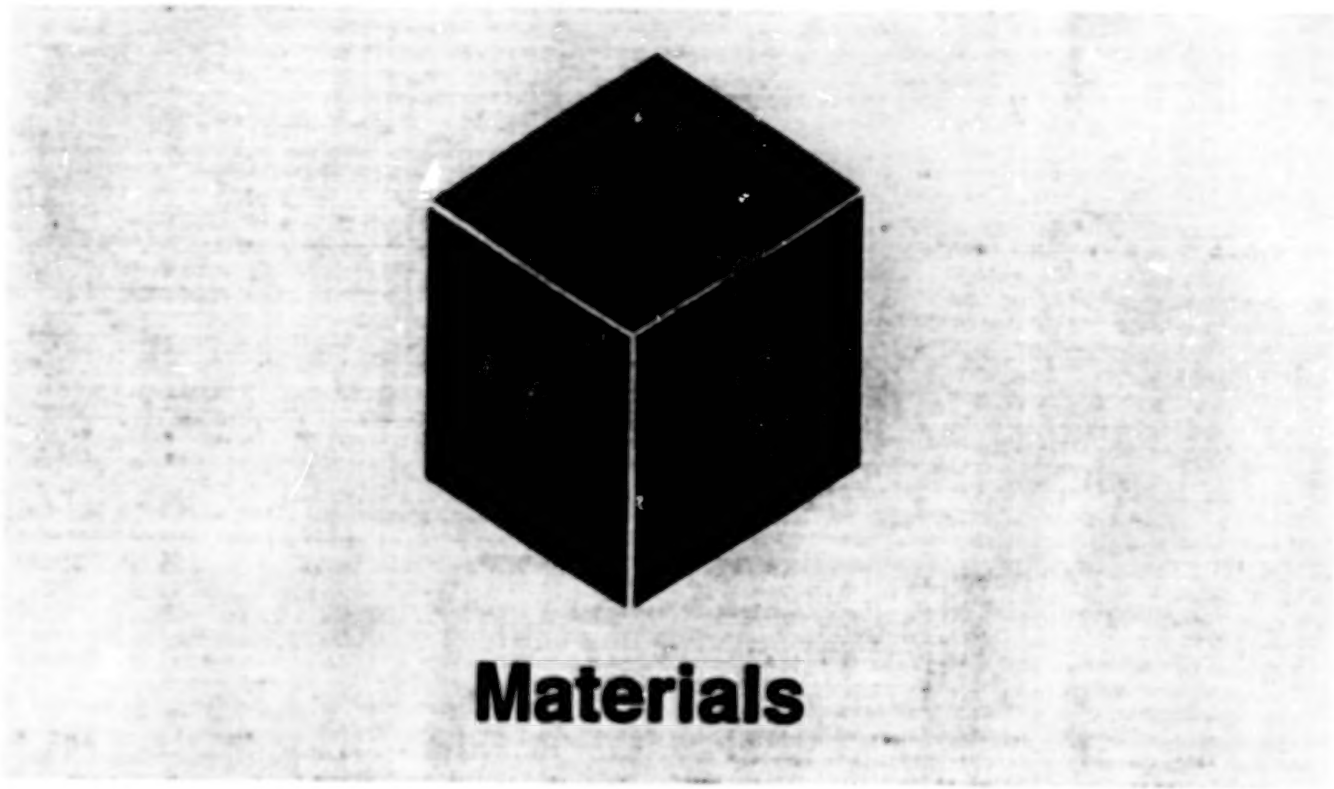

Materials

Hardware, Techniques, and Processes

28

BLANK PAGE

Polyorganosiloxanes for Coating Porous Ceramic Insulation

Protective coating and repairs can be performed relatively easily.

Ames Research Center, Moffett Field, California

Liquid and paste polyorganosiloxane formulations (which become high-temperature- and oxidation-resistant organosilicone-based ceramics upon curing) have been invented for use in (1) protecting porous, lightweight ceramic thermal insulation materials against aeroconvective thermal degradation and (2) repairing and bonding such materials. These formulations were originally intended especially for application to the fibrous refractory composite insulation (FRCI) tiles that protect parts of the space shuttles during reentry into the terrestrial atmosphere; they may also be suitable for application to similar insulating tiles in laboratory and industrial furnaces.

A formulation of this type starts out as a mixture of (1) one or more liquid di- and tri-functional organosilanes; (2) one or more suitable fillers to enhance chemical, mechanical, and/or thermal properties of the uncured mixture and/or the organosilicone end product; and (3) water. The functionality of the organosilanes resides in alkoxy groups attached to the silicon atoms. Before application to a ceramic thermal-insulation surface that one seeks to protect or bond, the mixture is allowed to cure partially at room temperature by the hydrolysis and partial condensation of the organosilanes with the water, yielding liquid polyorganosiloxanes (incompletely polymerized organosilicones) with unreacted silanol groups. Also formed in the condensation reaction are alcohols, which become dissolved in the remaining water. The resulting mixture can be applied to the surface of the ceramic insulation by spraying, brushing, rolling, flowing, or other conventional technique.

After application, the mixture is allowed to cure at room temperature to become a soft solid coat. The mixture continues to cure at room temperature, eventually becoming a hard polyorganosiloxane coat. The continued curing occurs by condensation of the unreacted silanol groups. If desired, curing can be accelerated by heating. When exposed to still higher temperature (especially in an extreme oxidative and aeroconvective environment like that experienced by a spacecraft during re-entry), the coat becomes an oxidation-resistant and thermally stable protective ceramic on the underlying ceramic insulation.

A low-viscosity, watery formulation of this type, with or without one or more fillers, would ordinarily be applied to a porous ceramic tile and allowed to soak into a surface layer of pores so that, upon curing, it could form a protective surface layer within and on the ceramic substrate to prevent the entry of hot gases. A viscous liquid formulation containing larger amounts of fillers could be applied to the surface of the ceramic tile to form a hard, impermeable layer on the external surface of the ceramic. A highly viscous formulation in the form of a paste could be suitable as an adhesive and/or filler for fabrication or repair. For example, the paste could be used to fill small holes caused by chipping or to cement plugs in place to fill larger holes (see figure).

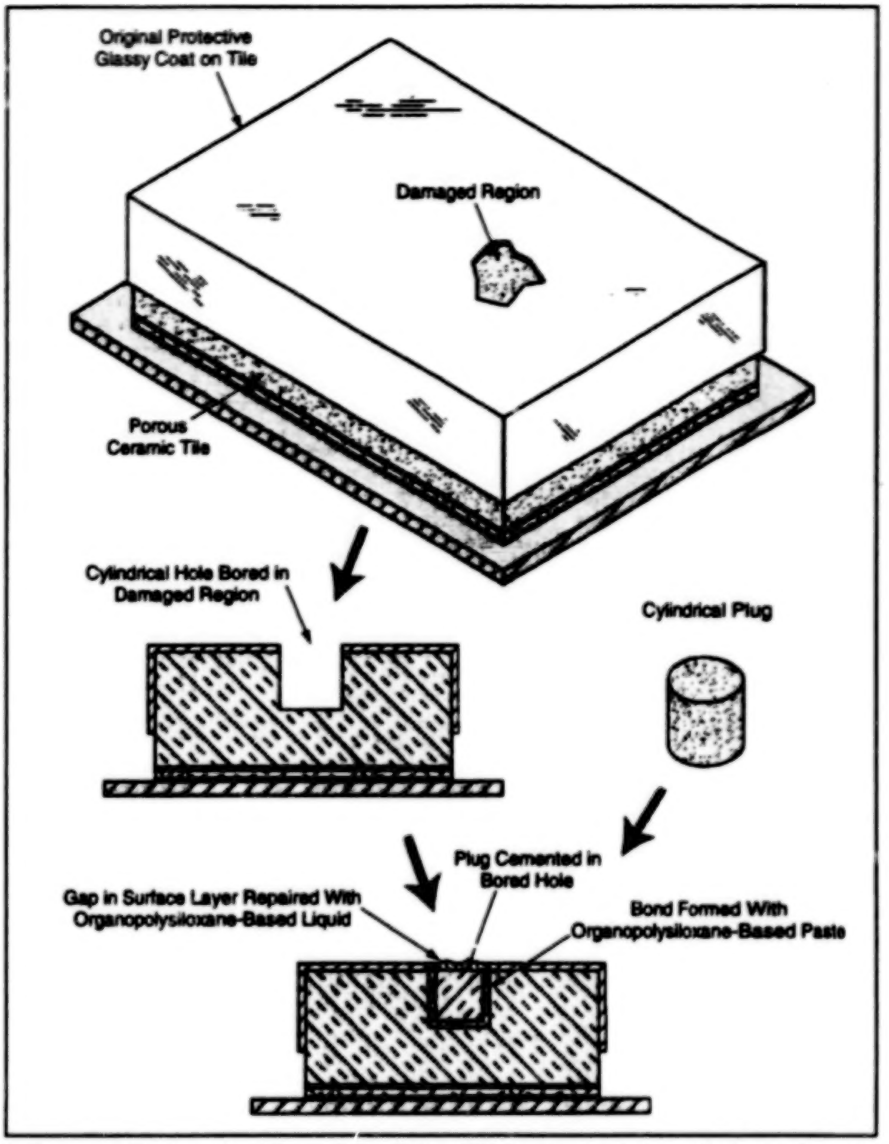

A Damaged Region of a Thermal-Insulation Tile is bored out to a cylindrical shape to receive a cylindrical repair plug. Prior to insertion of the plug in the hole, the side and bottom of the plug and/or the hole are coated with a viscous polyorganosiloxane-based adhesive. After insertion, the outer surface of the plug is coated with a dilute organopolysiloxane formulation to close the opening in the original glassy protective coat.

This work was done by Daniel B. Leiser, Ming-ta S. Hsu, and Timothy S. Chen of **Ames Research Center**. *Further information is contained in a TSP [see page 1].*

This invention has been patented by NASA (U.S. Patent No. 5,985,433). Inquiries concerning nonexclusive or exclusive license for its commercial development should be addressed to the Patent Counsel, Ames Research Center, (650) 604-5104. Refer to ARC-14077.

Attachment of Small SiC Hoops to SiC-Based Ceramics and Composites

These hoops can be used to hold sensor lead wires in place.

John H. Glenn Research Center, Cleveland, Ohio

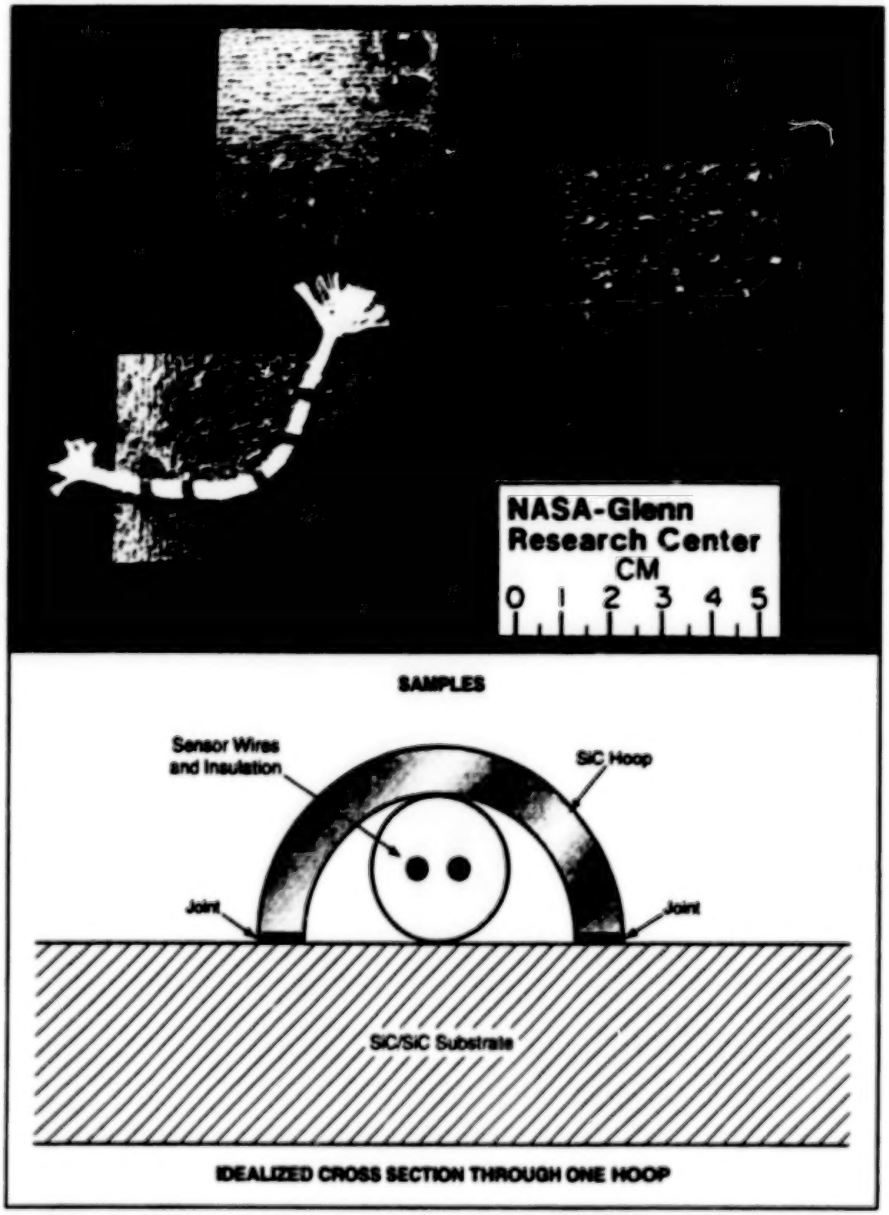

Semicircular SiC Hoops that have been reaction-bonded to SiC/SiC composite substrates are used to hold wires in place. The substrates shown here are flat, but the concept has also been demonstrated on curved substrates.

A technique for holding sensor lead wires in place on substrates made of SiC-based monolithic ceramic or SiC/SiC fiber-reinforced ceramic-matrix composite materials involves routing the wires through semicircular hoops that have been reaction-bonded to the substrates. These hoops are made of SiC-based materials similar or identical to the substrate materials. This technique was devised to prevent the detachment of lead wires from surface-mounted thin-film sensor systems (e.g., thermocouples and strain gauges) during testing of the substrates (panels, subcomponents, etc.) at temperatures >1,000 °C in the presence of high-speed gas flows.

The reaction-bonding process used to join the hoops to the substrates is called "ARCJoinT" (which signifies "Affordable, Robust Ceramic Joining Technology"). This process was described in several previous *NASA Tech Briefs* articles, including "Joining of SiC-Based Ceramic and Fiber-Reinforced Composite Parts" (LEW-16405), Vol. 22, No. 5 (May 1998), page 54; "Reaction-Forming Method for Joining SiC-Based Ceramic Parts" (LEW-16661), Vol. 23, No. 3 (March 1999), page 50; and "Reaction-Forming Method for Joining SiC-Based Parts" (LEW-16827), Vol. 24, No. 4 (April 2000), page 59. To recapitulate: A carbonaceous mixture is applied between the parts to be joined. The parts are heated to a temperature of 115±5 °C for 10 to 20 minutes. This action cures the mixture, bonding the parts with moderate strength. Next, silicon or a silicon alloy in tape, paste, or slurry form is applied to the joint regions. The parts are heated to a temperature between 1,250 and 1,425 °C for 5 to 10 minutes, causing the silicon to melt, infiltrate the joints, and react with carbon. The finished, full-strength joints contain silicon carbide with minor amounts of silicon and other phases. The joints are expected to retain mechanical strength and integrity at temperatures up to 1,350 °C in air.

Once hoops have been joined to a substrate via this approach, the sensor lead wires can be slipped through the hoops (see figure) and connected to the sensors. Any excess space between the lead-wire insulation and the hoop can be filled with a refractory cement or another nonreactive material, if necessary, to prevent the wires from moving.

As an alternative to SiC as a starting material, hoops could be made initially of carbon — more specifically, graphite. If carbon hoops are used, then additional silicon is applied to the joints and the carbon is converted to silicon carbide during the bonding process. The advantage of this approach is the relative ease of machining graphite (vs. machining SiC).

This work was done by J. Douglas Kiser, Jih-Fen Li, and Lisa C. Martin of **Glenn Research Center** *and Mrityunjay Singh of Dynacs Engineering Co. Further information is contained in a TSP [see page 1].*

Inquiries concerning rights for the commercial use of this invention should be addressed to NASA Glenn Research Center, Commercial Technology Office, Attn: Steve Fedor, Mail Stop 4–8, 21000 Brookpark Road, Cleveland, Ohio 44135. Refer to LEW-17009.

Polymer/Metal Laminate for Heat-Pipe and Radiator Envelopes

This material is durable, flexible, hermetic, and heat-sealable.

Lyndon B. Johnson Space Center, Houston, Texas

A thin polymer/metal laminate has been developed for use as an envelope material for lightweight heat pipes and heat-pipe radiators that operate at temperatures up to 360 K. The material is flexible enough to make it possible to roll or fold heat pipes compactly for transport and to unfurl them for use. The material is durable enough to withstand folding or rolling without incurring leaks. In addition, it is heat-sealable and thus an attractive alternative to metal heat-pipe envelope materials, which must be welded or brazed at temperatures much greater than those needed for heat sealing.

A polymer/metal laminate was selected for development because neither a metal nor a polymer foil exhibits the required properties, whereas the combination of materials could be expected to exhibit those properties. A metal foil can serve as a leak-proof pressure boundary for containing a heat-transfer fluid, but it fatigues easily and fails through growth of cracks and/or pinholes at the highly stressed tips of wrinkles that form during flexing. A polymer film has the required flexibility and does not develop cracks or pin holes when flexed; however, air and the vapor of the heat-transfer fluid can diffuse through a polymer film. When the two materials are bonded together in a laminate, the metal foil serves as the fluid-containment and pressure boundary, while the polymer film supports the metal foil, preventing large localized stresses and thus increasing the flex-fatigue resistance of the metal foil. With the proper selection of laminate layers, a laminate can be designed to exhibit such desired characteristics as flex-fatigue resistance, high emissivity, and resistance to ultraviolet radiation.

Material	Thickness of Layer, mm	Notable Characteristics of Layer Material
Polyvinyl Fluoride (Tedlar TWH15BL3 or Equivalent)	0.0380	Ultraviolet Diffuse Reflector, Emissivity = 0.826, Absorptivity = 0.383
Copper	0.0340	Roll-Annealed, Surface Treated With Electroplated Copper
Polyvinyl Fluoride (Tedlar TWH10BS3 or Equivalent)	0.0254	High Yield Elongation, Low Moisture Transmission
Copper	0.0340	Roll-Annealed, Impermeable, Strong
Polyvinyl Fluoride (Tedlar TWH10BS3 or Equivalent)	0.0254	High Yield Elongation, Low Moisture Transmission
Polypropylene	0.0952	Very High Yield Elongation, Negligible Moisture Transmission, Heat-Sealability

This Six-Ply Polymer/Metal Laminate offers a combination of flexibility, strength, and thermal stability not available from any of the laminate materials taken by itself. The laminate has an overall thickness of 0.252 mm and an areal mass density of 40 g/ft^2 (0.43 kg/m^2).

The present laminate contains six plies. It is an improved derivative of four-ply polymer/metal laminates that are used commercially to package foods and medicines and that do not have the strength or the high-temperature stability required for the heat-pipe application.

The table describes the six layers. The two copper layers provide the hermetic seal; in contrast, all commercial laminates use only single metal layers. The use of two metal layers in this laminate affords redundancy for protection in the event that a leak arises in one metal layer. The innermost layer is made of a heat-sealable polymer to ease fabrication. The outer polyvinyl fluoride layer provides the optical properties needed for efficient radiation of heat.

This work was done by John D. Cornwell of **Johnson Space Center** *and John E. Fale and Nelson J. Gernert of Thermacore, Inc. Further information is contained in a TSP [see page 1].*

MSC-22856

Improved Polymeric Composite Materials for Dental Fillings

In comparison with prior formulations, these materials shrink less.

Lyndon B. Johnson Space Center, Houston, Texas

Composite materials that include combinations of metal oxide and silica nanoparticles in polymeric matrices have been invented for primary use as dental fillings, dental and bone adhesives, and the like. There have been previous efforts to develop polymeric replacements for the amalgam used traditionally as dental filling material, but those efforts involved polymers that exhibited unfavorable characteristics, including shrinkage and poor adhesion to bone. Strong adhesion is desirable and zero shrinkage is essential for a dental filling material because accumulated stresses from shrinkage can cause debonding with consequent leakage and attack by microbes. The present materials are formulated to obtain stronger adhesion and less shrinkage.

A somewhat detailed presentation of historical and technical background is prerequisite to a meaningful description of the invention. One polymeric material that had been suggested previously for use in dental fillings is made from the monomer bis-glycidylmethylmethacrylate (bis-GMA). The use of bis-GMA together with other ingredients usually included in dental adhesives or fillings yields materials with desirable physical properties, but these materials exhibit considerable post-shrinkage and adhere poorly to teeth.

Other polymeric filling materials also exhibit less than the desired amounts of adhesion to tooth surfaces. In order to obtain desired bonding on enamel or dentin, the protein coatings on the enamel or the smear level on the dentin must be removed. Traditionally, this has been done by use of such organic acids as phosphoric, citric, lactic, and diamine dicarboxylic acid. Thus, many tooth-filling products contain polyacids as surface-cleaning and priming agents for enamel and dentin. Because bis-GMA is not inherently adhesive to tooth surfaces, similar provisions for etching by acids would have to be made if bis-GMA were to be used.

Another class of candidate dental adhesive and filling materials includes some nematic liquid crystals that can be

photopolymerized within seconds, at temperatures in the vicinity of 90 °C. These materials form densely cross-linked networks of reaction extent greater than 95 percent and exhibit very little polymerization shrinkage because of the high packing efficiency that already obtains in the nematic state. However, polymerization at lower temperatures (including room temperature) results in undesirable intervening smectic and crystalline phases that make the materials unsuitable as medical and dental restoratives. This completes the background information.

In a representative composite material of the present invention, the matrix resin preferably consists of, or at least includes, an acrylate or methacrylate-based nematic liquid-crystal monomer that is photopolymerizable at room temperature and exists in the nematic state (with suppression of crystallinity) at room temperature. The resin is formulated to be able to accommodate a high loading of metal oxide or metal oxide and silica nanoparticles, to enable the resin/particle mixture to flow when pushed into cavities to be filled, and to form a high-molecular-weight polymer, with little or no shrinkage upon polymerization.

The metal oxide and silica nanoparticles help to provide strength. The metal oxide particles can also be used to impart opacity for x-ray photography. While any metal capable of forming one or more amphoteric oxide(s) could be used, tantalum is particularly advantageous for imparting x-ray opacity to the composite.

For compatibility with teeth, the metal oxide particles must not exhibit high surface acidity. The surface acidity of tantalum oxide nanoparticles is neutralized by mixing, with the particles, a polymerizable, biocompatible, heterocyclic base (e.g., an alkene-terminated imidazole or phosphate) that can form complexes with the acid sites on the surfaces of the particles.

In many cases, it is desirable to formulate resin/nanoparticle filling mixtures to be translucent or transparent. In a typical dental restorative procedure, a liquid or pasty filling material is placed on a tooth and ultraviolet light used to effect the polymerization (cure) into a high-strength, hard, x-ray-opaque coating or filling, with essentially zero shrinkage. The transparency or translucency makes it possible to effect photopolymerization of a thicker layer of filler than would otherwise be possible, thus making it unnecessary to apply and photocure multiple thinner layers.

This work was done by Stephen T. Wellinghoff of Southwest Research Institute for **Johnson Space Center**. *Further information is contained in a TSP [see page 1].*

In accordance with Public Law 96-517, the contractor has elected to retain title to this invention. Inquiries concerning rights for its commercial use should be addressed to

Stephen T. Wellinghoff
Southwest Research Institute
6220 Culebra Road
Drawer 28510
San Antonio, TX 78228

Refer to MSC-22842, volume and number of this NASA Tech Briefs *issue, and the page number.*

Polyorganosiloxane Waterproofing for Porous Ceramics

Relatively nontoxic coating materials can be applied and cured easily.

Ames Research Center, Moffett Field, California

Liquid waterproofing agents based on polyorganosiloxanes have been invented for use in treating porous, lightweight, fibrous ceramic thermal-insulation materials in both tile (rigid) and blanket (flexible) forms. Whereas silane-based waterproofing materials developed previously for this purpose are toxic and volatile and must be applied in tedious procedures (involving repeated injection at multiple locations by use of syringes), the present formulations are nontoxic and nonvolatile and can be applied by ordinary coating procedures.

Waterproofing of lightweight, fibrous ceramic thermal-insulation materials is needed for the following reasons: These materials are often hygroscopic. Because of its porosity and hygroscopicity, such a material can absorb as much as five times its own weight in water. In addition to adding unacceptably to the weight of the insulation, absorbed water could give rise to freeze/thaw damage or to damage from explosive vaporization upon sudden exposure to very high temperature.

A waterproofing agent of the present type is formulated as an aqueous solution of di- and tri-alkoxyfunctional organosilanes, the molecules of which contain hydrocarbyl groups of between 1 and 10 carbon atoms. The functionality resides in alkoxide groups attached to the silicon atoms. Before application to a ceramic thermal-insulation material, the solution is allowed to cure partially at room temperature by the hydrolysis and partial condensation of the organosilanes with the water, yielding low-molecular-weight polyorganosiloxanes with unreacted silanol groups. Also formed in the condensation reaction are small amounts of alcohols, which become dissolved in the water. If desired, alcohol can be added to the solution to facilitate drying; however, it has been found that the addition of water alone yields satisfactory results. Thus, unlike previously developed waterproofing materials, which generally contain such toxic, volatile solvents as toluene, xylene, naphtha, and/or lacquer thinner, this waterproofing agent is relatively nontoxic and nonvolatile.

The resulting solution can be applied to the ceramic insulation that one seeks to render waterproof by any suitable conventional coating technique — for example, spraying, brushing, rolling, or flowing. The solution penetrates the ceramic substrate to some depth by capillary action in the pores. Thus, what is formed is not a continuous coat on the exterior surface that would seal against penetration of all liquids and gases; instead, the interior surfaces of the pores become coated with a thin layer of waterproofing material that adds little to the overall weight of the ceramic. The waterproofing treatment is completed by mild heating (typically to no more than about 100 °C) to drive the condensation reaction to completion and to dry the coated ceramic substrate. Heating can be effected by use of a heat gun, heat lamp or any other convenient means.

This work was done by Daniel B. Leiser, Domenick E. Cagliostro, Ming-ta S. Hsu, and Timothy S. Chen of **Ames Research Center**. *Further information is contained in a TSP [see page 1].*

This invention has been patented by NASA (U.S. Patent No. 5,766,322). Inquiries concerning nonexclusive or exclusive license for its commercial development should be addressed to the Patent Counsel, Ames Research Center, (650) 604-5104. Refer to ARC-14068.

Hybrid Composite Structures Made From Polybenzoxazole Fibers

Strength-to-thickness ratios would be increased.

NASA's Jet Propulsion Laboratory, Pasadena, California

Hybrid composite-material (fiber/matrix) structures of a proposed type would incorporate recently developed polybenzoxazole (PBO) fibers that feature high strengths and high moduli of elasticity and which can be made in much thinner sections than are possible with graphite fibers. The PBO fibers could be used, for example, in skins, face sheets, or panels, any or all of which could be made as multiple-angle-ply layups.

In comparison with similar structures made from graphite fibers to satisfy a given set of strength and stiffness requirements, those made from PBO fibers to satisfy the same set of requirements could be thinner. In a typical application, PBO-fiber laminated face sheets or skins would be bonded to graphite stiffeners or honeycomb cores to make hybrid composite stiffened sandwich structures thinner and less massive than the corresponding structures made with graphite (only) fibers, due to the thinner sections possible with PBO fibers.

This work was done by Joseph Lewis of Caltech for **NASA's Jet Propulsion Laboratory**. *Further information is contained in a TSP [see page 1].*

NPO-20774

BLANK PAGE

Computer Programs

Mathematics and Information Sciences

BLANK PAGE

Mathematics and Information Sciences

Program for Evaluating Spacecraft Designs and Missions

Design for X (DFX) is a computer program that assists, at the preliminary stage of planning, in the evaluation of alternative spacecraft designs and mission scenarios. The input required by DFX includes a set of operations goals (scientific and engineering goals and constraints), a mathematical model of the spacecraft, and a set of scoring functions for quantifying the engineering utility and/or scientific value of various operations. DFX uses the operations-goals and model information, along with artificial-intelligence-based planning and scheduling techniques, to generate a high-level activity plan that is then scored by the provided functions. The benefits of using DFX to automate the evaluation of spacecraft designs include (1) improved scientific spacecraft design, leading to improved science return; (2) greater accuracy in analysis of margins and interactions, leading to improved operability of the spacecraft; and (3) decreased project risk (e.g., budget and schedule risk) from rapid prototyping and analysis of designs.

This program was written by Robert Sherwood, Gregg Rabideau, Steve Chien, and Tobias Mann of Caltech for **NASA's Jet Propulsion Laboratory**. *Further information is contained in a TSP [see page 1].*

This software is available for commercial licensing. Please contact Don Hart of the California Institute of Technology at (818) 393-3425. Refer to NPO-20492.

Programming Language for Automated Scheduling and Planning

The ASPEN Modeling Language (AML) has been developed for use in the Automated Scheduling and Planning Environment (ASPEN) software system. As described in prior *NASA Tech Briefs* articles, ASPEN is an object-oriented system that contains a modular, reconfigurable, reusable set of components that implement the elements commonly found in complex automated-scheduling application programs. AML has a simple syntax that makes it easy for a user who lacks expertise in computer science and artificial intelligence to rapidly create a model of a spacecraft-operations domain for an ASPEN automated-scheduling application program. AML enables a user to construct a model, expressed as a plain-text file, that defines activities, resources, and states. A user can also modify a model without need to recompile ASPEN. AML encodes spacecraft operability constraints, flight rules, spacecraft hardware models, goals of scientific experiments, and operational procedures to enable the generation, by the automated-scheduling program, of low-level sequences of spacecraft operations.

This program was written by Robert L. Sherwood, Alex Fukunaga, David Yan, Quoc Vu, Gregg Rabideau, Steve Chien, and Anita Govindjee of Caltech for **NASA's Jet Propulsion Laboratory**. *Further information is contained in a TSP [see page 1].*

This software is available for commercial licensing. Please contact Don Hart of the California Institute of Technology at (818) 393-3425. Refer to NPO-20281.

Communication Software for Distributed Application Programs

The Task Remote Asynchronous Message Exchange Layer (Tramel) software reduces the costs of distributing application programs across computer networks, including the Internet. Tramel implements robust, reliable, simple, highly portable interprocess communication, such that distributed application programs can tolerate extreme deterioration of communication links and elements of such a program can be stopped, moved to other computers (including computers with different operating systems), and restarted, all while the program is running and without alteration of any source code or configuration file. Because Tramel is based on asynchronous message passing, it can tolerate extremely low link performance without sacrificing transaction concurrency or relying on a multithreading system. Tramel manages network connections for an application program, shielding the program from such details as processor architectures, operating systems, and communication protocols. At the same time, Tramel affords monitoring capabilities that can keep application-program elements informed of the current configuration of the program. Tramel can be executed on any of a variety of computers running the UNIX, VxWorks, or Windows NT operating system.

This program was written by Scott Burleigh of Caltech for **NASA's Jet Propulsion Laboratory**. *Further information is contained in a TSP [see page 1].*

This software is available for commercial licensing. Please contact Don Hart of the California Institute of Technology at (818) 393-3425. Refer to NPO-19889.

Software for Coordinating Multiple Exploratory Robots

A computer program coordinates the activities of multiple instrumented robotic vehicles of the "rover" type intended for use in scientific exploration. The program is a master/slave, distributed version of the ASPEN planning software, other versions of which have been reported in several prior *NASA Tech Briefs* articles. On the basis of an input set of goals and the initial conditions of each rover, the program generates a sequence of activities that satisfy the goals while obeying the resource constraints and rules of operation of each rover. The program includes a central planning subprogram that assigns goals to individual rovers in such a way as to minimize the total traversal time of all the rovers while maximizing the scientific return. The remainder of planning is distributed among the individual rovers: each rover runs a subprogram that plans its activities to attain the goal(s) assigned to it.

This program was written by Tara Estlin, Darren Mutz, Steve Chien, Anthony Barrett, and Gregg Rabideau of Caltech for **NASA's Jet Propulsion Laboratory**. *Further information is contained in a TSP [see page 1].*

This software is available for commercial licensing. Please contact Don Hart of the California Institute of Technology at (818) 393-3425. Refer to NPO-21031.

Program Creates Code to Parse Text

Savj is a computer program that facilitates the development of programs that parse textual input in the Java programming language. Savj is a parser generator that creates static Java parsers in the

same sense in which YACC, Bison, and YACC++ are static parser generators that create static C-language parsers. Saxj creates Java object-oriented parsers on the basis of grammar specifications. Saxj uses an algorithm of the "look-ahead 1 token, look right" [LALR(1)] type to convert a grammar specification into a parser. Saxj is built upon implementation of this algorithm by use of a library of Java classes. Grammar specifications in Saxj are intentionally similar to those in YACC, Bison, and YACC++, so that the documentation of Saxj can be nearly the same as that of YACC++. The various instantiations of the class of parsers contain a single definition of the parse table; it is in this sense that the parsers are characterized as static. All of the parsers generated by the YACC family are similarly static. A dynamic parser is feasible in the case of machine learning. Saxj can be used, for example, for writing compiler software, for interpreting sequences of computer-generated commands, and for general language parsing.

This program was written by Richard Weidner of Caltech for **NASA's Jet Propulsion Laboratory**. *Further information is contained in a TSP [see page 1].*

This software is available for commercial licensing. Please contact Don Hart of the California Institute of Technology at (818) 393-3425. Refer to NPO-21055.

Program Creates Java Lexical Analyzers

Luthorj is a computer program that creates static lexical analyzers in the Java programming language, in the same sense in which Flex and Lex create lexical analyzers in the C programming language. The majority of users of Luthorj are expected to be familiar with Lex, and Luthorj parses input files that are largely the same as Lex files. However, Luthorj is not merely a look-alike, Java version of Lex. The functionality of Luthorj is partly compatible with that of Flex, but Luthorj and Flex use different methods to provide similar functionality. The lexical analyzers created by Luthorj convert textual strings into tokens that, in turn, can be fed to parsers created by the Saxj program described in the preceding article. Luthorj converts input string specifications to lexical-analysis data structures by use of an algorithm that converts regular expressions to nondeterministic finite automata (NFA). The NFA are then mapped to deterministic finite automata (DFA). The combination of all DFA are represented as a transition table, which is stored in a file. The outputs of Luthorj are the transition table and the code to use it.

This program was written by Richard Weidner of Caltech for **NASA's Jet Propulsion Laboratory**. *Further information is contained in a TSP [see page 1].*

This software is available for commercial licensing. Please contact Don Hart of the California Institute of Technology at (818) 393-3425. Refer to NPO-21054.

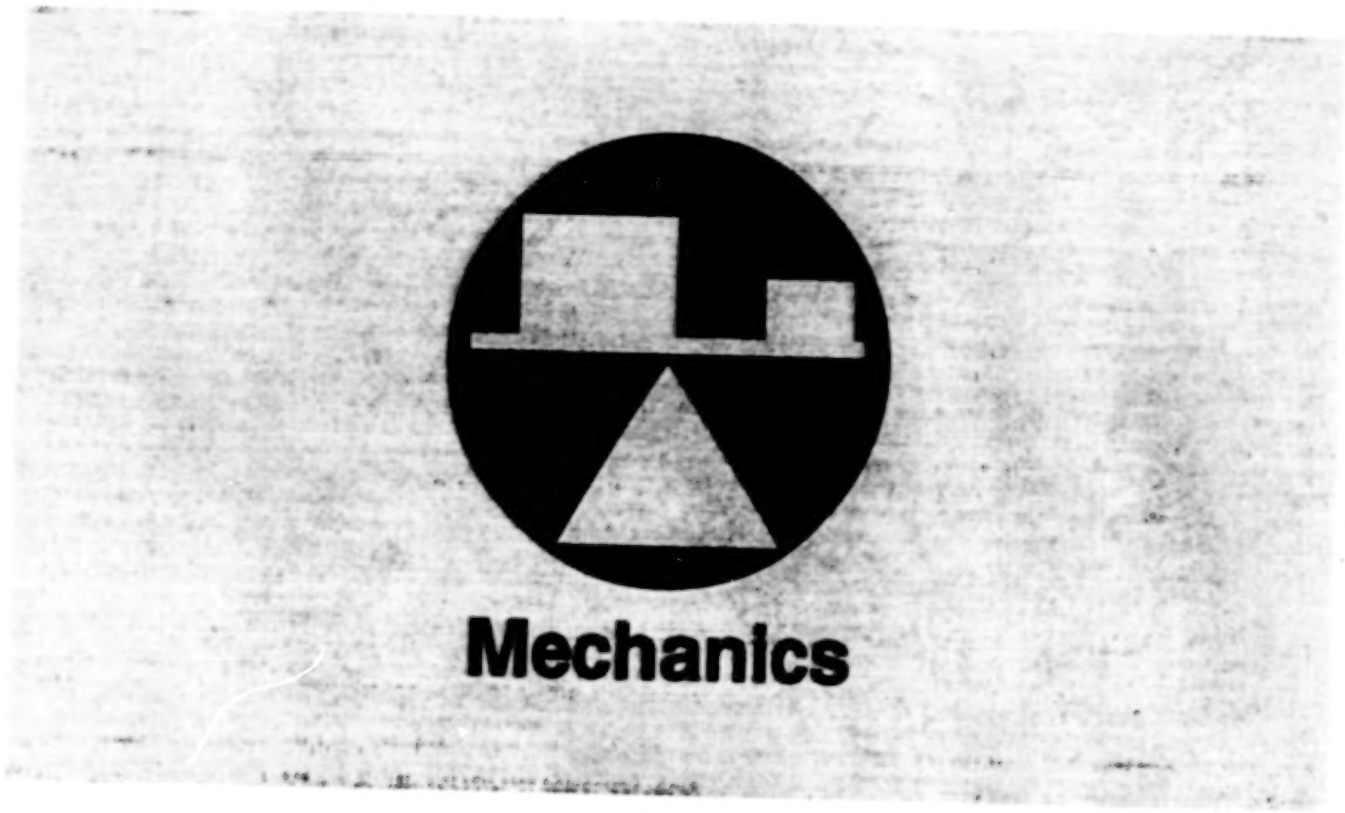

Hardware, Techniques, and Processes

BLANK PAGE

Micromachined Double Resonator

The design affords both vibration isolation and low-loss suspension.

NASA's Jet Propulsion Laboratory, Pasadena, California

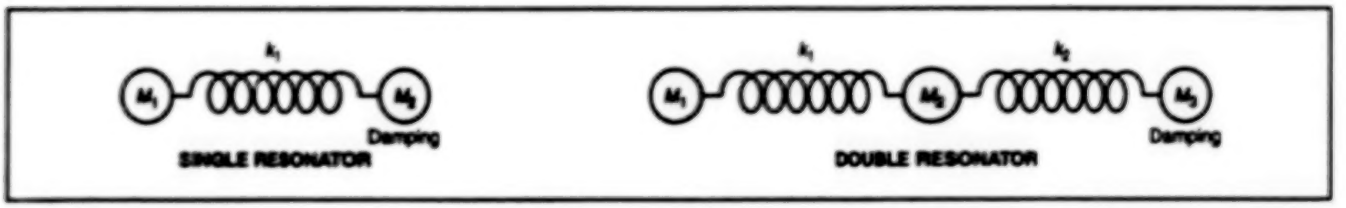

Simple Mass/Spring/Damper Models are used to compute the resonance frequencies and *Q* values of the single- and double-resonator designs.

A double-resonator design has been devised for a cloverleaf-shaped silicon microelectromechanical resonator. The double-resonator design provides for an inner, higher-frequency resonator suspended on an outer, lower-frequency resonator. This design concept affords several advantages, as described below.

A typical prior design of a microelectromechanical resonator calls for a solidly mounted substrate. Solid mounting entails (1) poor vibration isolation and (2) high energy losses in the substrate, with consequent decrease of the resonance quality factor (*Q*). The double-resonator design was inspired by the realization that solid mounting is not necessarily desirable and that if the substrate of a resonator is suspended on thin springs, what is formed is a double-mass resonator that can have a *Q* greater than that of the original resonator. In addition, the outer resonator helps to isolate the inner resonator from packaging stresses and from vibrations of external origin.

The figure schematically depicts mathematical models of the previous single-resonator design and the present double-resonator design. The schematic diagrams reflect the observation that it is more accurate to model the substrate as a finite mass with damping than to assume that the substrate is so rigidly mounted that it represents an infinite mass. In the single-resonator design, resonator mass M_1 is coupled, via a spring of stiffness k_1, to a damped substrate mass M_2. This model yields close agreement between predicted and measured *Q* factors.

In the double-resonator design, inner resonator mass M_1 is suspended on a spring of stiffness k_1 that is attached to an intermediate mass M_2, which, in turn, is coupled to damped substrate mass M_3 via a spring of stiffness k_2. M_2 is chosen to be much greater than M_1; consequently, the frequency and mode shape of the higher-frequency (M_1,k_1,M_2) resonance does not differ greatly from that of the single-resonator design. M_3 is also chosen to be much greater than M_1; this choice, in combination with the choice of M_2, and with the choice of k_1 and k_2 to be approximately equal, ensures that the damping on M_3 exerts little effect on the *Q* of the higher-frequency resonance.

Because of the isolation provided by k_2, very little of any mounting stress that might be imposed on M_3 is coupled into k_1. In addition, because of the largeness of M_2 relative to M_1, very little of any vibration imposed on M_3 propagates to M_1. Another advantage of the double-resonator design is that M_2 can be tailored to exert a slight effect on the resonances (in other words, to tune the vibrating system); it is easier to tune in this way that to tailor k_1.

In the prototype double resonator, the substrate of a cloverleaf resonator substructure is suspended by four springs that connect it to an outer frame. The lowest resonance frequency of the cloverleaf is designed to be 6 kHz, while the lowest resonance frequency for vibration isolation is designed to be 200 Hz. It has been predicted that the cloverleaf resonance will have a $Q > 10^4$, and that because of damping in the outer frame, the substrate resonance will have $Q < 100$.

This work was done by Roman Gutierrez, Tony K. Tang, and Kirill Shcheglov of Caltech for **NASA's Jet Propulsion Laboratory.** *Further information is contained in a TSP [see page 1].*

In accordance with Public Law 96-517, the contractor has elected to retain title to this invention. Inquiries concerning rights for its commercial use should be addressed to

Technology Reporting Office
JPL
Mail Stop 122-116
4800 Oak Grove Drive
Pasadena, CA 91109
(818) 354-2240

Refer to NPO-20658, volume and number of this NASA Tech Briefs *issue, and the page number.*

Mechanical Breakaway Clutch

A proposed mechanical breakaway clutch would not rely on friction. The clutch would be useful in environments in which the inherent inaccuracies of friction would make friction clutches erratic. The proposed clutch would comprise two primary assemblies: a driver assembly and a slip flange. The slip flange would be an internally splined cup driven by the driver assembly. The driver assembly would feature a sliding spring that would provide full adjustability. Roller bearings could be used to deflect the spring simultaneously as they were forced inward by the splines of the slip flange. In an alternate configuration, rotating cams would be used in place of the ball bearings. By varying the linear position of the spring assembly, one could adjust the level of torque at which the clutch would slip.

This work was done by Jeffrey K. Hostetler of **Johnson Space Center.** *Further information is contained in a TSP [see page 1].*

MSC-22506

BLANK PAGE

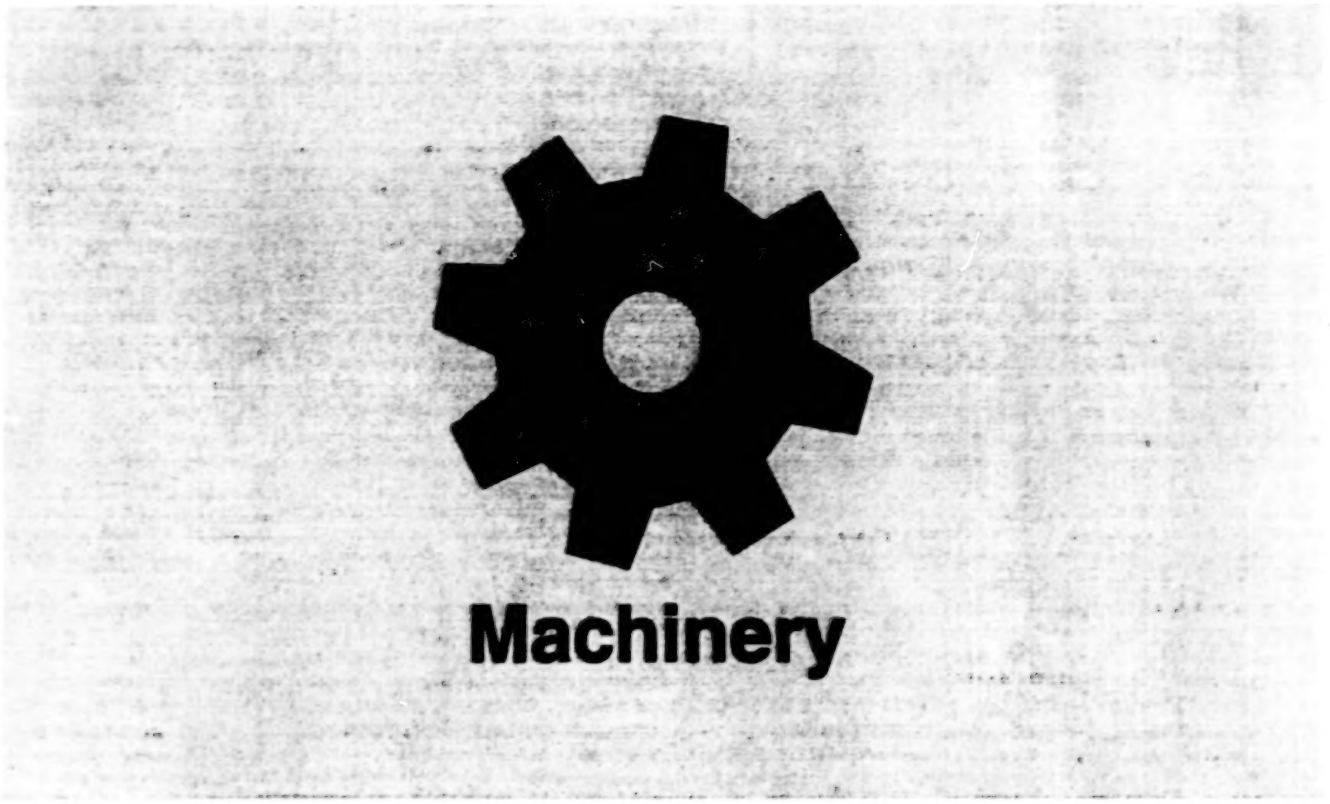

Machinery

Hardware, Techniques, and Processes

BLANK PAGE

Water-Jet/Ultrasonic Removal and Real-Time Gauging of Paint

Ultrasound would loosen paint, and sensory feedback would guide the paint-removal apparatus.

NASA's Jet Propulsion Laboratory, Pasadena, California

An improved robotic water-jet system for stripping paint from a ship or other large metallic structure is undergoing development. In addition to utilizing a high-pressure water jet to remove paint and a robotic crawler to scan the jet along the painted structure, the system utilizes high-intensity ultrasound to loosen the paint just ahead of the water jet in order to ensure more nearly complete removal. The improved system also includes a quantitative gauging subsystem that measures the thickness of the paint and a qualitative gauging subsystem that generates an approximate map of paint residues; these subsystems provide real-time feedback for control of the crawler, water-jet, and ultrasonic subsystems.

The ultrasonic subsystem exploits a combination of heating and mechanical stresses to loosen paint. In the focal zone, the intense ultrasound can raise the temperature several hundred degrees, causing the paint to blister. In the presence of the mismatch of acoustic impedances between the paint and the metallic substrate, the ultrasound gives rise to tensile and shear stresses that contribute to blistering. The paint is further damaged if ultrasonic cavitation is present.

The ultrasonic paint-loosening subsystem includes a piezoelectric transducer that generates focused ultrasonic waves; the transducer is mounted on the crawler and positioned to concentrate the ultrasound into the surface layer of water on the workpiece near the advancing water jet (see Figure 1). The transducer is excited with a combination of two ultrasonic signals — one at a frequency of several hundred kilohertz (chosen for its shorter wavelength and thus greater amenability to focusing) and one at a frequency of tens of kilohertz (chosen because it is more effective in producing cavitation in water). The more highly focused higher-frequency ultrasound propagates into the lower-frequency ultrasonic field, raising the intensity of the total ultrasonic field in the focal region above the threshold for cavitation (U.S. Pat. No. 5,827,204.)

Two candidate transducer concepts for the quantitative thickness-gauging subsystem have been identified. The first concept is that of an eddy-current thickness gauge: one would place a small electromagnet coil in contact with the paint, excite the coil with alternating current at a suitable frequency, measure the impedance of the coil, and deduce the thickness of paint from the known variation of impedance of the coil with distance from the metal substrate.

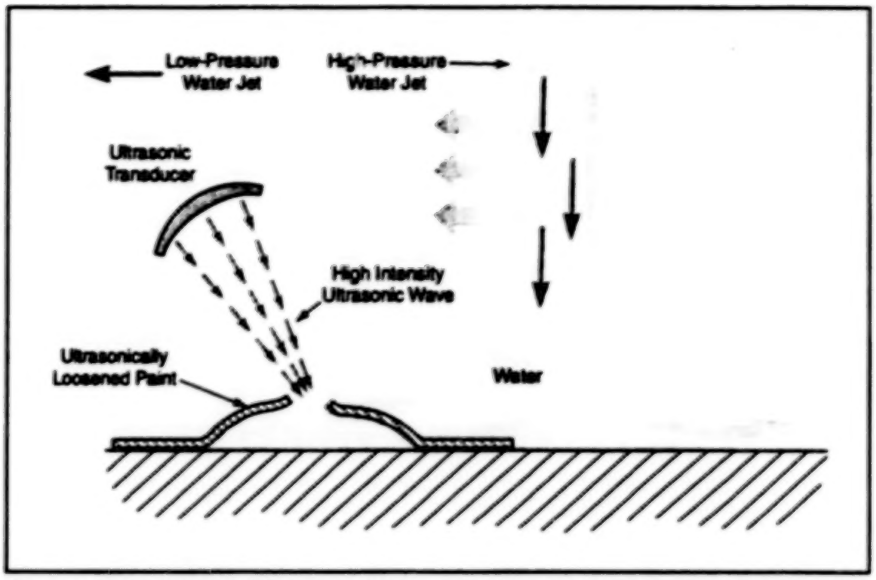

Figure 1. Concentrated Ultrasound blisters and otherwise loosens paint, facilitating the removal of the paint by a high-pressure water jet.

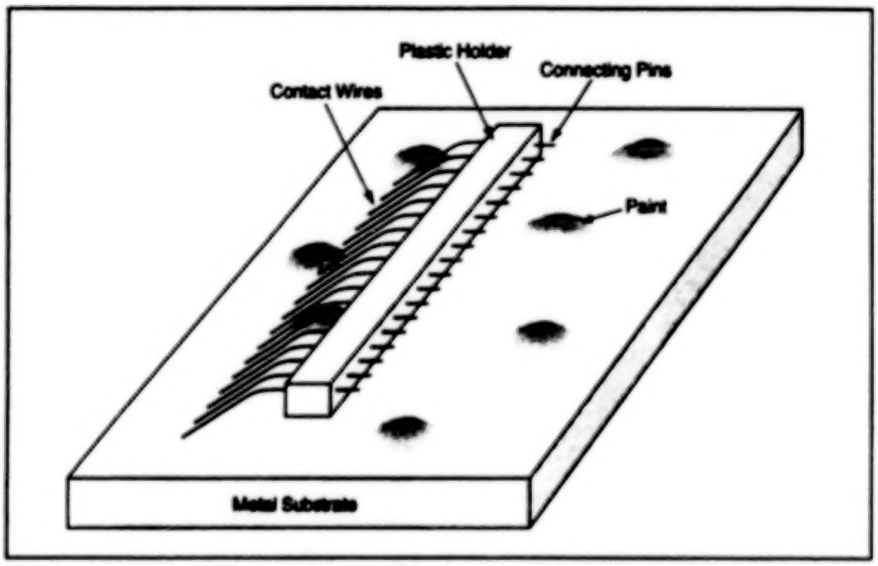

Figure 2. A Comb of Springy Contact Wires is scanned along the workpiece to test for removal of paint, as indicated by electrical continuity between the wires and the metal substrate.

The second transducer concept is that of an ultrasonic thickness gauge that would give a direct reading of the thickness of the paint. This gauge would include ultrasonic transducers operating in the frequency range of 1 to 10 MHz. The high-pressure water jet would be used as the coupling medium. It would be necessary to compensate the gauge reading for the effects of stripped paint and bubbles. Rapid spectral analysis could be used to reduce the effects of noise and interference.

The qualitative thickness-gauging subsystem would include a comb array of springy wire electrodes that would be scanned along the workpiece behind the water jet. The number of wire electrodes would be chosen to obtain the desired resolution. By simple electrical contact (or lack thereof) with the metal substrate, the electrodes would give indications of the removal or nonremoval of paint from their respective

locations. In real time, contact/noncontact signals from the wires could be multiplexed and sent as feedback to a control subsystem. For non-real-time inspection, contact/noncontact signal data acquired by scanning along the workpiece could be used to generate a map of paint residues.

This work was done by Yoseph Bar-Cohen, Xiaoqi Bao, and Neville Marzwell of Caltech for **NASA's Jet Propulsion Laboratory**. *Further information is contained in a TSP [see page 1].*

In accordance with Public Law 96-517, the contractor has elected to retain title to this invention. Inquiries concerning rights for its commercial use should be addressed to

Technology Reporting Office
JPL
Mail Stop 249-103
4800 Oak Grove Drive
Pasadena, CA 91109
(818) 354-2240

Refer to NPO-21063, volume and number of this NASA Tech Briefs issue, and the page number.

Molten-Carbonate Oxidation of Solid Waste

This process is relatively safe and efficient.

Lyndon B. Johnson Space Center, Houston, Texas

The molten-carbonate oxidation (MCO) process shows promise as a means of safe disposal and/or recycling of solid waste. The MCO process is being developed for use in regenerative life-support systems in outer space, but may also prove useful in managing institutional, industrial, and/or municipal solid waste. The MCO process completely oxidizes wastes as diverse as polytetrafluoroethylene, polyvinyl chloride, polyethylene terephthalate, polyethylene, feces, wheat straw, and cellulose. An MCO system can operate at atmospheric pressure without flames and without direct feed of fuel into the oxidation chamber — all important safety features.

In the MCO process, a mixture of approximately equimolar proportions of sodium carbonate and potassium carbonate is melted and heated to a temperature between 800 and 900 °C. The waste to be oxidized is fed into the melt. Oxygen or air is also fed into the melt. The chemical environment in the carbonate melt favors the formation of superoxide ions (O_2^-), which catalyze oxidation of the waste. The result is a kinetically rapid three-dimensional homogeneous reaction in which the solid waste is converted to carbon dioxide and water vapor, which bubble away from the melt and can be reclaimed. Any inorganic materials in the waste are converted to minimal amounts of ashes and/or to inorganic salts, which can be removed by a commercial salt-splitting unit and reused.

Typically, the melt is contained in a stainless-steel or alumina tank. Both the oxidizing gas and the waste feed are introduced into the melt from the bottom: This practice forces the waste and gas to rise through the full depth of the melt, maximizing contact between the waste and the molten-salt mixture and thereby the degree and the overall rate of oxidation of the waste.

The melt is heated initially and thereafter maintained at the required high temperature by use of an electric furnace. Inasmuch as most wastes are low-grade fuels, the oxidation of the waste supplies some heat, thereby reducing the electric power needed to maintain the high temperature. The consumption of energy can be reduced further by efficient insulation of the tank and/or furnace and by regenerative recovery of heat from the reaction products.

The MCO equipment is relatively simple, with few moving parts. Pretreatment of waste is not strictly necessary, although some milling of the waste feedstock can be beneficial. The flow of oxidizing gas and the proportion of nonexothermic material in the waste feed can be adjusted to help keep the temperature of the melt in the desired range.

This work was done by G. Duncan Hitchens and Oliver J. Murphy of Lynntech, Inc., for **Johnson Space Center**. *Further information is contained in a TSP [see page 1].*

MSC-22467

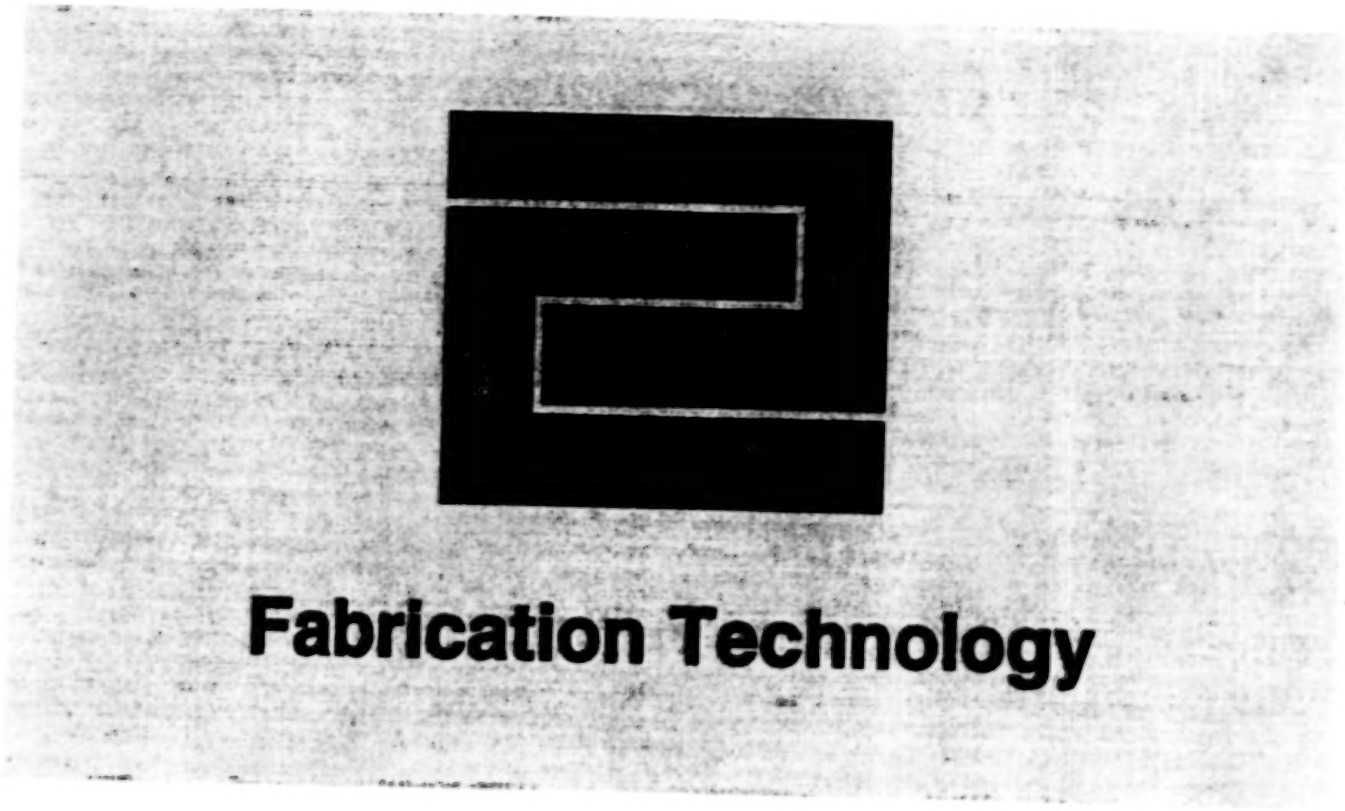

Fabrication Technology

Hardware, Techniques, and Processes

BLANK PAGE

Hermetic Wafer Bonding by Use of Microwave Heating

Clamping is unnecessary, and the only appreciable heating occurs in the metal bond.

NASA's Jet Propulsion Laboratory, Pasadena, California

Microwave heating is the basis of a simple technique for quickly and gently bonding two metallized dielectric or semiconductor wafers to each other. The technique can be used, for example, to bond a flat, gold-coated silicon wafer to another gold-coated silicon wafer that is flat except for a cavity, in order to hermetically seal the cavity (see figure). The technique has the potential to become a standard one for bonding in the fabrication of microelectromechanical systems (MEMS).

The predecessor of this technique is thermocompression bonding, in which two substrates to be bonded are clamped together with considerable pressure and the entire resulting assembly is heated to melt eutectic metal alloy coats on the faying substrate surfaces. (Even though elemental metals could be more desirable under some circumstances, eutectics are used because they have lower melting temperatures.) The bonding process can take as long as 24 hours. The heat and pressure can degrade the product; the degradation can include deleterious effects of clamping stresses, diffusion of the metal into the substrate material, and diffusion of substrate material into the metal bond.

In the present technique, bonding could be effected in a few seconds, with minimal or no clamping, and without heating the entire assembly. Two pieces to be bonded are simply placed (e.g., one atop the other), in a microwave cavity. The position and orientation of the pieces in the microwave cavity is chosen to optimize coupling of the metal in the bond with the electromagnetic mode that is to be excited in the microwave cavity. The microwave cavity is evacuated to prevent the formation of a plasma. A pulse of microwave power (typically a few hundred watts for a few seconds) is applied.

Because the substrates are nearly transparent to microwaves in the presence of metal layers, heating by the microwave field is concentrated in the metal layers in the bond region. More precisely, by virtue of the electromagnetic skin effect, most of the deposition of electromagnetic energy occurs within a skin depth (≈1 μm at microwave frequencies) at the surface of the metal. Thus, heating is concentrated exactly where it is needed — at the interface between the two metal layers that one seeks to melt together. By the time the pulse is turned off, the metal layers have been melted together, yet the substrates remain cool. Of course, heat is conducted from the interface to adjacent depths, but the resulting heating of the substrate is transient and minimal — not enough to cause appreciable diffusion of metal or substrate material.

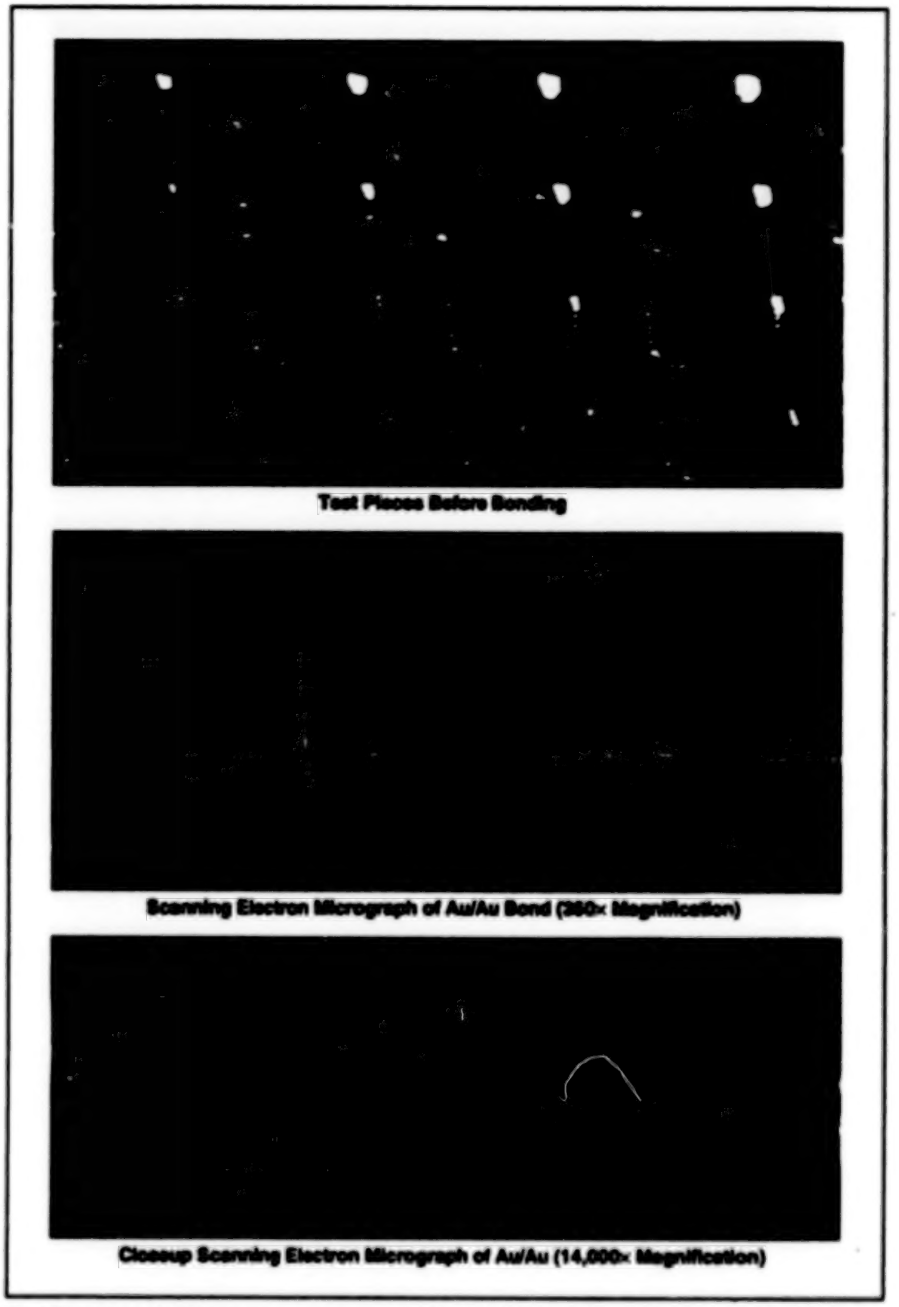

Test Pieces containing square recesses were bonded to form hermetically sealed rectangular parallelepiped cavities. The closeup micrograph clearly shows the fusion of metallic layers.

The figure depicts some aspects of silicon workpieces that were fabricated and tested to demonstrate the present technique. Each piece started as 5-mm square silicon wafer. A strip 2 mm wide around the edge of one face of each piece was coated with Cr to a thickness of 150 Å, then Au to a thickness of 1,200 Å. The gold coat was to serve later as the bonding metal. Each piece was etched to form 3-by-3-mm, 100-μm-deep recess in the middle of one face; the recess was to become half of a hermetically sealed cavity. Then pairs of these pieces were bonded to form the hermetically sealed cavities. In a test of their

hermeticity, the bonded pairs were found to leak at low rates comparable to the background level of a leak-measuring mass spectrometer.

This work was done by Nasser Budraa, Martin Barmatz, John Mai, Tom Pike, and Henry Jackson of Caltech for **NASA's Jet Propulsion Laboratory**. *Further information is contained in a TSP [see page 1].*

This invention is owned by NASA, and a patent application has been filed. Inquiries concerning nonexclusive or exclusive license for its commercial development should be addressed to the Patent Counsel, NASA Resident Office–JPL [see page 1]. Refer to NPO-20608.

Chemical Machining of Microscopic Holes and Grooves in Glass

This technique overcomes disadvantages of conventional macro- and micromachining.

NASA's Jet Propulsion Laboratory, Pasadena, California

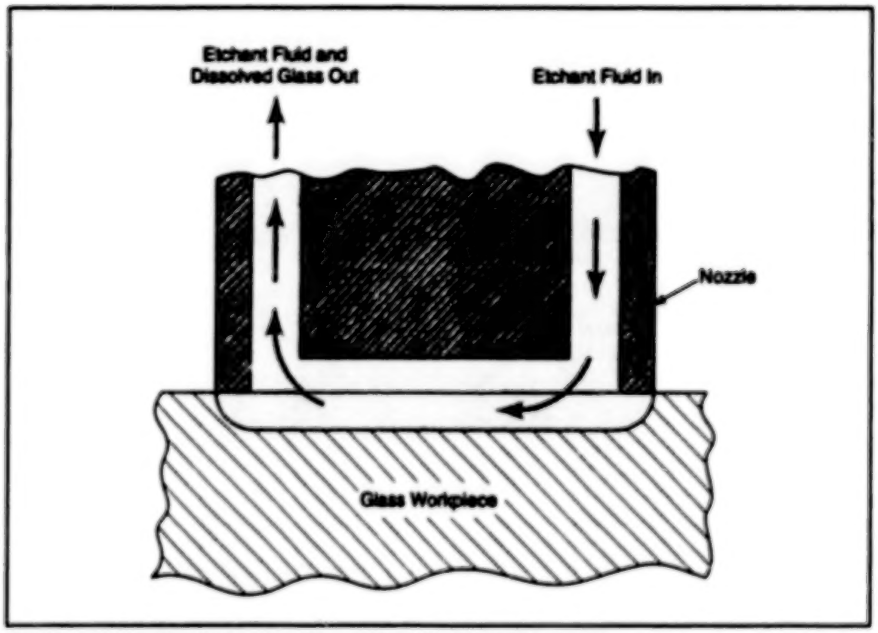

Etching Is Localized along the flow path at the tip of the nozzle.

A technique for making precise, microscopic holes and grooves in glass workpieces has been invented. The technique differs from both (1) traditional macroscopic mechanical drilling and milling and (2) conventional micromachining that involves etching through photolithographically patterned masks. The technique can be used, for example, to make holes between 20 μm and 1 mm in diameter.

The technique involves wet chemical etching, but unlike in conventional micromachining, the etch is localized. As shown in the figure, a hole in a glass workpiece is formed by use of a nozzle that contains at least one delivery channel and at least one return channel for the flow of an etchant fluid. Both channels open out to the tip of the nozzle. By use of a pressure pump at the far end of the delivery channel and/or a suction pump at the far end of the return channel, the etchant fluid is made to flow across the tip of the nozzle. The flowing etchant dissolves and carries away the glass along the flow path in the tip region. Unlike in conventional machining, the surface of the workpiece does not become roughened by abrasion, and there is no contamination by particles of workpiece material.

The shape and width of the resulting hole or groove is determined by the size and shape of the nozzle. As etching proceeds, the nozzle is either moved deeper into the workpiece to deepen the hole or else moved laterally (along the surface of the workpiece) to lengthen the groove. The nozzle can be fabricated, to the required precision, by use of photolithography and deep trench etching. The movement of the nozzle can be automated easily with computerized control. The precision of the movement, and thus of the final product, can be as high as 1 μm; such a level of precision has been demonstrated in robotic equipment commonly used in micromachining in a clean room.

This work was done by Kirill Shcheglov and William Tang of Caltech for **NASA's Jet Propulsion Laboratory**. *Further information is contained in a TSP [see page 1].*
NPO-20732

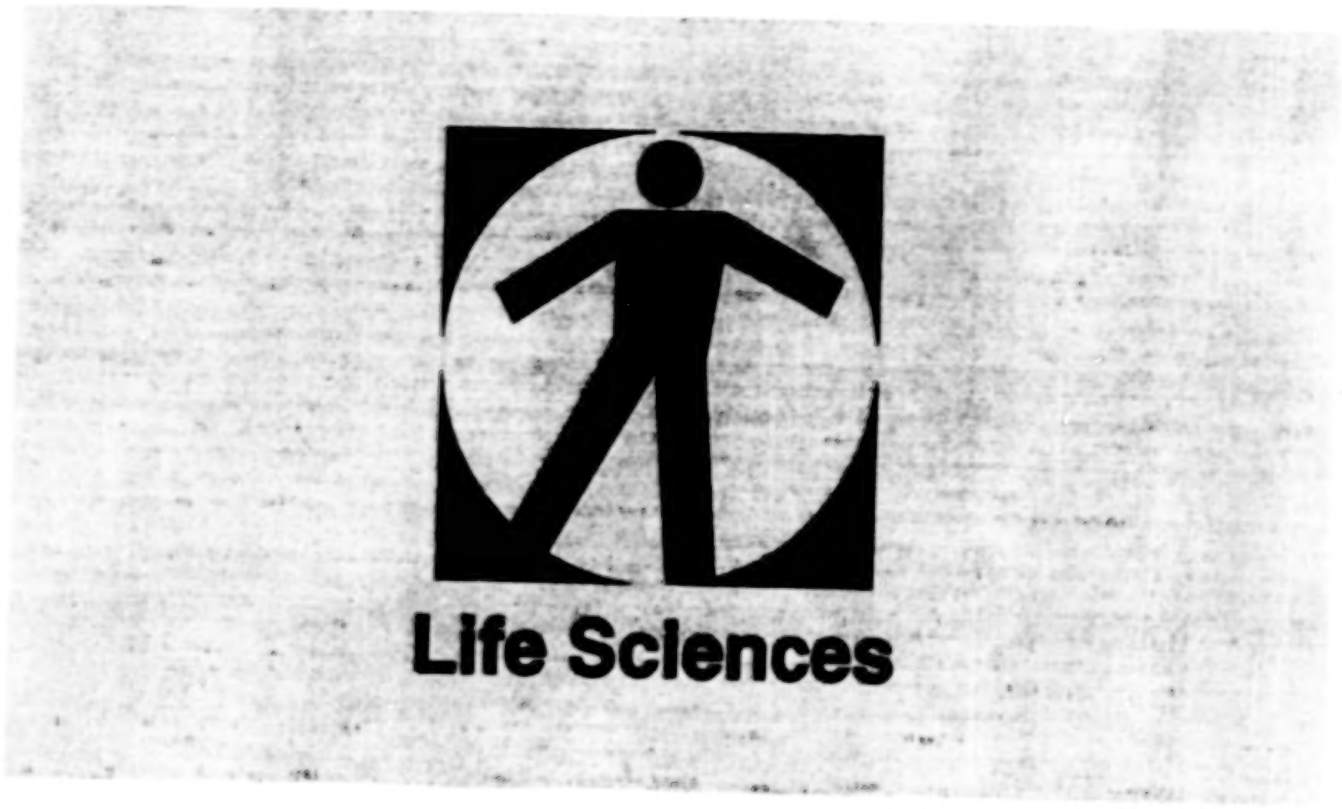

Hardware, Techniques, and Processes

BLANK PAGE

Macroextraction for Purification of Nucleic Acids

Nucleic acids can quickly be extracted from relatively large volumes of starting materials.

Lyndon B. Johnson Space Center, Houston, Texas

A technique for extracting samples of ribonucleic acid (RNA) and deoxyribonucleic acid (DNA) for use in diagnosing and studying infectious and genetic diseases has been developed. The technique enables the concentration and purification of nucleic acids from large (in comparison with older techniques) volumes of bodily fluids or digested tissues, with minimal nuclease activity and minimal loss of the nucleic acids.

The technique involves the use of a centrifuge equipped to handle 15-milliliter polypropylene conical tubes that are standard equipment items in biomedical research. Fresh or frozen samples with volumes up to 4 milliliters can be used without prior concentration steps and without numerous microfuge tubes; these features minimize the loss of nucleic acids and the cross-contamination of samples, both of which are observed when numerous concentration steps and numerous tubes are used. Isolation of DNA and/or RNA can be accomplished in as little time as 40 minutes.

The technique involves the use of an extraction solution of the following composition:

- 1 part by volume of a solution that has a pH of 7.0 and that contains (a) guanidinium thiocyanate at a concentration 4 M, (b) sodium citrate at a concentration of 25 mM, (c) sarcosyl at a concentration of 0.5 percent by volume, and (d) 2-mercaptoethanol at a concentration of 0.1 M;
- 0.1 part by volume of a 0.2-M solution of sodium acetate;
- 1 part by volume of an aqueous solution of phenol at a pH of 7.9; and
- 0.2 part by volume of chloroform.

The following are the steps of the extraction procedure according to this technique:

1. Add the extraction solution to each sample.
2. Transfer the entire volume sample (usually 2 to 3 mL) of each sample to one of the 15-mL polypropylene conical tubes.
3. To each such tube, add 2.5 mL of RNAzol™ and 0.25 mL of R-chloroform, then vortex for 20 seconds.
4. Put each such tube on ice for ten minutes.
5. Spin the tubes in the centrifuge at a speed that yields a centripetal acceleration of 10,000 times normal Earth gravitation for 10 minutes.
6. Take the top layer of each sample that has been centrifuged, add an equal volume of isopropyl alcohol, and vortex briefly.
7. Let each such sample stand for at least 2 hours at a temperature of -20 °C to allow precipitation to take place. Alternatively, faster precipitation of nucleic acids can be achieved through addition of ammonium acetate.
8. Perform centrifugation (again at 10,000 times normal Earth gravitation) for 10 minutes on the samples that have undergone the precipitation treatment.
9. Remove and discard the liquid from each sample, which now takes on the form of a pellet.
10. Wash each pellet by gently overlaying it with an aqueous solution of 75 percent ethanol.
11. Decant the liquid.
12. Use a disposable laboratory towel wrapped around forceps to wipe, from inside each sample tube, the solid sample material left behind by decanting of the liquid.
13. Resuspend the solid material in 30 µL of a buffer solution of 1x tris-ethylenediaminetetraacetic acid (EDTA).

This work was done by Duane L. Pierson of **Johnson Space Center** *and Raymond P. Stowe. Further information is contained in a TSP [see page 1].*

MSC-22841

"Breathprint" Analysis of Microbial Communities

A technique for assessing changes in the densities and compositions of communities of microorganisms in environmental samples is based partly on redox chemistry. Suspensions of microbes from environmental samples are inoculated into 95-well microtiter plates. Each well contains an initially colorless redox-sensitive dye and a source of carbon different from the sources of carbon in the other wells. If the microorganisms in a well can utilize or degrade the source of carbon, then the colorless dye is reduced to a colored crystal. The overall pattern of color in the various wells can be regarded as a "breathprint" of the microbial community. Because inoculation of the wells takes less than a minute and the reading of colors and analysis of the resulting data are largely automated, an assay by this technique can be performed relatively quickly. The technique has been used for such diverse purposes as monitoring the stability of microbial populations in artificial plant-growth and life-support systems, testing for toxicity, monitoring bioremediation, monitoring industrial bioreactors, studying subsurface microbiology, and studying fertility of agricultural soils.

This work was done by John Sager of **Kennedy Space Center** *and Jay L. Garland of the Dynamac Corp. Further information is contained in a TSP [see page 1].*

Inquiries concerning rights for the commercial use of this invention should be addressed to the Technology Programs and Commercialization Office, Kennedy Space Center, (407) 867-6373. Refer to KSC-12065.

END

12-4-01